Linking Root System Architecture (RSA), Photosynthetic Efficiency, and Biomass Productivity in a Switchgrass (Panicum virgatum L.) Half-Sib Panel

Jazib Ali Irfan
University of Georgia
Shiva Om Makaju
University of Georgia
Ali Mekki Missaoui
cssamm@uga.edu

University of Georgia

Research Article

Keywords: Switchgrass, Functional phenomics, Gas exchange, Intrinsic water-use efficiency, Root system architecture (RSA), Chlorophyll fluorescence

Posted Date: February 17th, 2026

DOI: https://doi.org/10.21203/rs.3.rs-8734576/v1

Additional Declarations: No competing interests reported.

Title: Linking Root System Architecture (RSA), Photosynthetic Efficiency, and Biomass Productivity in a Switchgrass (*Panicum virgatum* L.) Half-Sib Panel

Jazib Ali Irfan[1,2], Shiva Om Makaju[1,2,3], Ali Mekki Missaoui[1,2,3]*

[1]Institute of Plant Breeding, Genetics, and Genomics, University of Georgia, Athens, GA 30602, USA

[2]Center for Applied Genetic Technologies, University of Georgia, Athens, GA 30602, USA

[3]Department of Crop and Soil Sciences, University of Georgia, Athens, GA 30602, USA

***Correspondence:** Ali Mekki Missaoui (cssamm@uga.edu)

Abstract

Switchgrass (*Panicum virgatum* L.) is a perennial forage crop for renewable fuel production. However, biomass yield is a complex trait shaped by physiological and root characteristics. We tested whether switchgrass families with contrasting multi-year biomass performance exhibit differences in leaf gas exchange parameters, chlorophyll fluorescence, and seedling root system architecture (RSA). Leaf gas exchange was assessed by comparing top- and low-yielding families using analysis of covariance (ANCOVA) of net CO_2 assimilation (A) against stomatal conductance (g_{sw}), including group × g_{sw} interaction. Chlorophyll *a* fluorescence was evaluated using rapid light curve (RLC)-derived OJIP induction metrics. Seedling RSA was quantified in rhizoboxes using RhizoVision analysis and complementary manual measurements of roots and shoots. Top-yielding families maintained higher A at comparable g_{sw} (group effect = 5.50, P = 0.00247), and showed a weaker dependence of A on g_{sw} (interaction estimate = –18.685, P = 0.00703), consistent with greater photosynthetic capacity and tighter stomatal regulation. Intrinsic water-use efficiency (iWUE) varied, with the highest iWUE values confined to top-yielding

families, and a quantile-regression upper envelope indicating a carbon-water trade-off at high A. In contrast, OJIP metrics such as electron transport rate (ETR), maximum quantum efficiency of photosystem II (Fv/Fm), and performance index (PIabs) were similar between yield groups (median initial slope, α = 0.081–0.082). Seedling RSA exhibited strong root-shoot coordination but showed weaker associations with field biomass within the top group (r = –0.35 to –0.41). Overall A–g_{sw} and iWUE patterns were informative of field biomass than seedling RSA or chlorophyll fluorescence alone.

Panel on the left side shows the methodology of data collection using LI-6800 and HANDY PEA on the field at IHF.

Seeds from the parent populations were used to evaluate the root morphology and aboveground biomass features among rhizobox grown progeny population.

The effective way of linking above-ground biomass yield to overall root morphological characteristics, and photosynthetic performance of the mature stands.

Keywords: Switchgrass; Functional phenomics; Gas exchange; Intrinsic water-use efficiency; Root system architecture (RSA); Chlorophyll fluorescence.

Glossary

A – Net CO_2 assimilation rate

ANCOVA – Analysis of covariance

BLUP – Best linear unbiased predictions

C_i – Intercellular CO_2 concentration

C_a – Ambient CO_2 concentration

C_i/C_a – ratio of intercellular to ambient CO_2

ETR – Electron transport rate

E – Transpiration rate

Fv/Fm – Maximum quantum efficiency of PSII

g_{sw} – Stomatal conductance to water vapor

iWUE – Intrinsic water-use efficiency (A/g_{sw})

LatHFlux – Latent heat flux

LUE – Ligh-use efficiency

OJIP – Fast chlorophyll a fluorescence transient (O-J-I-P steps)

PAR – Photosynthetically active radiation

PIabs – Performance index (absorption basis)

PSII – Photosystem II

RLC – Rapid light curves

RSA – Root system architecture

VPD – Vapor pressure deficit

Introduction

Perennial C_4 grasses such as switchgrass (*Panicum virgatum* L.) are central to the sustainable bioenergy and forage production because they combine high biomass yield with relatively low input requirements and substantial below-ground carbon storage. It was adopted as a model herbaceous species by the U.S. Department of Energy's bioenergy program after multi-site evaluations showed that two major lowland and upland ecotypes of switchgrass can produce higher biomass on marginal lands [1]. A recent study conducted at Tifton, GA, identified accessions with improved drought adaptation [2], and a study conducted in Knoxville, Tennessee, identified accessions with improved nitrogen-use efficiency [3]. The work demonstrated that meaningful physiological variation exists within breeding germplasm and can be captured using BLUP-based indices. Beyond the use as bioenergy feedstocks and forage for livestock, perennial biomass crops such as switchgrass contribute to climate mitigation by sequestering soil organic carbon (SOC). Meta-analyses indicate that switchgrass and Miscanthus cultivation on marginal land enhances SOC stocks and promotes microbial-derived carbon formation compared with annual cropping [4]. Long-term experiments on perennial biomass systems further show that, with adequate establishment, these energy crops can accumulate more SOC than row crops, with the magnitude dependent on species and management [5]. Improvements in soil aggregate stability, enzyme activity, and other soil health indicators have also been reported under perennial biofuel crops on degraded soils [6]. While these ecosystem benefits are substantial, sustained adoption of perennial switchgrass as a bioenergy crop ultimately depends on stable and high biomass yield under variable environments.

Switchgrass has been widely evaluated for biomass yield potential on marginal lands across the United States, with substantial genetic variation reported for phenology, stress adaptation and

overall aboveground biomass yield [7, 8]. Screening of diverse germplasm has revealed families that differ markedly in drought responses, including gas exchange, osmotic adjustment, and metabolite profiles, highlighting the potential to breed for improved resilience [9]. Agronomic surveys emphasize that switchgrass has a deep, fibrous root system that extracts water from considerable depth and can use it more efficiently than many C_3 forage grasses [10]. Ecological assessments of natural and planted stands show that contrasting ecotypes and management regimes produce distinct patterns of spread and competitive ability [11]. Field studies under rainfed conditions support the view that switchgrass maintains leaf photosynthesis and growth during moderate drought relative to other perennial species [12]. At the same time, work on cadmium stress in seedlings demonstrates significant genetic variation in water-use efficiency (WUE) and stomatal regulation between upland and lowland types, implicating WUE genes as breeding targets [13].

Root system architecture (RSA) is central to the performance of perennial grasses. Deep-rooted crops can deliver water and nutrients from subsoil layers, enhance subsoil carbon storage and contribute to long-term carbon sequestration [14]. Studies of deep-rooted perennials show that they alter vertical patterns of microbial respiration and SOC chemistry, increasing plant-derived carbon at depth [15]. Perennial grass systems are increasingly recognized as economically viable carbon sinks when managed for both grain or forage and ecosystem services [16]. In mixed warm-season grass swards, inclusion of C_4 species has been associated with increased root biomass and below-ground carbon, especially during warm seasons [17]. At broader spatial scales, grassland syntheses indicate that soil carbon stocks covary closely with below-ground biomass across precipitation and temperature gradients [18]. Ten-year comparisons of perennial versus annual cropping systems

116 further document shifts in enzyme activities and carbon fractions under tall fescue and grass-
117 legume mixtures, underscoring the functional importance of roots in soil carbon dynamics [19].
118 At the leaf level, net CO_2 assimilation (A), stomatal conductance (g_{sw}), and intrinsic water-use
119 efficiency (iWUE = A/g_{sw}) integrate biochemical capacity and stomatal behavior [20]. Analyses
120 of natural variation show that iWUE differs among families, seasons and environments, and can
121 help dissect trade-offs between carbon gain and water conservation [21]. In Sorghum, diversity
122 panels reveal substantial genetic variation in transpiration efficiency and WUE that underpins
123 adaptation to water-limited production systems [22]. Crop-scale modelling work indicates that
124 WUE is tightly linked to light-use efficiency and evaporative demand, implying that selection on
125 leaf gas-exchange traits must be interpreted in the context of canopy light interception [23].
126 Process-based simulations also highlight that improving WUE is necessary but not sufficient to
127 sustain yields in water-limited regions [24].
128 Functional phenomics has emerged as a framework that couples high-throughput phenotyping with
129 physiology to understand how trait variation drives performance in complex environments [25].
130 Root functional phenomics extends this framework below-ground using imaging-based platforms
131 to quantify RSA at scale [26]. Recent reviews emphasize that shoot and root phenotyping
132 increasingly relies on imaging, robotics, and machine learning to capture responses to abiotic stress
133 across large populations [27]. The RhizoVision platform, for example, enables standardized
134 analysis of root images from rhizoboxes and soil cores for phenotypic and genetic studies [28]. In
135 parallel, active chlorophyll fluorescence techniques enable rapid in situ measurement of
136 photosystem II (PSII) function for precision agriculture and stress monitoring [29]. The
137 chlorophyll *a* fluorescence induction (OJIP)-based fluorescence analyses have been applied in
138 perennial forage grasses such as ryegrass, tall fescue, and smooth brome to track seasonal

dynamics of photosynthetic activity and antioxidant capacity [30]. Yet work on winter hardiness and freezing tolerance showed that PSII-based indices such as maximum quantum efficiency of photosystem II (Fv/Fm) are not always straightforward predictors of yield and their utility can be species and year-dependent [31].

However, few studies have evaluated whether physiological and root traits measured at the leaf or seedling stage consistently align with multi-year, multi-location biomass performance in breeding-relevant switchgrass populations. There is a need for integrative studies that relate RSA, leaf photosynthesis, WUE/iWUE, and biomass yield performance within realistic breeding populations of perennial grasses such as switchgrass. In this study, we used top- and low-yielding half-sib family (progeny) groups, defined by previously predicted yield performance derived from a diverse switchgrass panel to test whether families selected for contrasting yield classes differ systematically in gas exchange, chlorophyll fluorescence, and seedling RSA. The objectives of this study were to identify physiological and architectural signatures associated with superior biomass yield and to assess the predictive value of seedling traits for mature stand performance by combining multi-year field data with LI-6800 gas exchange measurements, HANDY PEA-driven OJIP analyses, and RhizoVision-based root phenotyping.

Materials and methods

Experimental design and half-sib population development

The trials for this study were established in Knoxville, Tennessee, and in Georgia at two farm/sites. The initial polycross parent population was chosen from the diversity panel at Tifton [2]. The half-sib progeny population was established as described in our recently published work by Irfan, Makaju [32]. The published work by Irfan, Makaju [32] also provides details on the progeny

development, management, the land area required, mating design, field layout and statistical framework used to generate robust multi-environment yield estimates for family classification.

Biomass yield

The field biomass yield was quantified across three consecutive years (2022-2024) and two locations (Watkinsville, GA, and Tifton, GA). For each half-sib family/genotype, biomass yield was first summarized within each environment (location × year) using plant-level observations from the replicated field trials. Environment-specific adjusted means were then obtained using a linear mixed model including fixed and random effects with half-sib families treated as random effects. Treating families as random effects allowed estimation of performance that generalizes beyond individual site-year conditions. The mean field-evaluated yield used for downstream analyses and for defining yield classes was computed as the average of the environment-specific adjusted means across all available environments [32], thereby representing broad, multi-environment performance rather than a single site-year yield evaluation. Based on that multi-environment mean yield performance, the families were grouped into top- and low-yielding classes for physiological and phenomics comparisons.

Rapid light curves (RLC) and leaf-level gas exchange measurements

The present study used data collected exclusively at the Iron Horse Plant Sciences Farm (IHF), Watkinsville, GA (33.72458° N, -83.30262° W). The 50 best-performing half-sib progenies based on prior biomass performance (Top 50) and low-performing progenies (Low 50) were selected to evaluate the utility of functional phenotyping in switchgrass. Data for rapid light curves (RLCs) measuring photosynthetic efficiency were collected using a chlorophyll fluorometer, the HANDY Plant Environment Analyzer (HANDY PEA, Hansatech Instruments, Ltd., Norfolk, UK) [33]. Leaf gas exchange measurements were conducted on a subset of

established progeny plants at IHF, using the LI-6800 Portable Photosynthesis System (LI-COR Biosciences, Lincoln, NE, USA). Each family was replicated twice, corresponding to two field replicates (200 progenies). Measurements were taken on fully sun-exposed leaves in the upper canopy on clear days in mid-June 2025 between 09:00 and 16:00 h under ambient field conditions. The reference CO_2 concentration in the cuvette was maintained at 430 µmol mol^{-1} with a total flow rate of about 640 µmol s^{-1}. The photosynthetic photon flux density incident on the leaf surface was set to 1400 µmol m^{-2} s^{-1} using the integrated light source. The leaf temperature typically remained near 32 ºC to 33 ºC. The chamber humidity was adjusted so that the leaf-to-air vapor pressure deficit was generally close to 1.5-2.0 kPa. The instrument was configured to log steady-state gas exchange after a 15-second averaging period, recording net CO_2 assimilation rate (A), stomatal conductance to water vapor (g_{sw}), transpiration rate (E), intercellular CO_2 concentration (C_i), and associated environmental variables for subsequent analysis with biomass and root system architecture traits.

Seedling establishment in rhizoboxes

To proceed with growing seedlings in glass rhizoboxes, based on the progeny performance data for biomass yield from a three year biomass yield data across Watkinsville and Tifton in Georgia, 30 top-performing and 30 low-performing half-sib parents were selected out of 200 half-sib polycross parents, and seeds were de-husked using a laboratory seed debearder (Mater seed debearder, OEM, Inc., Corvallis, OR). The de-husked seeds were placed on water-soaked filter paper in petri dishes and covered with water-soaked filter paper. The lids of petri dishes were placed on top and sealed with parafilm. Seeds were then pre-chilled in a refrigerator for seven days to break seed dormancy. After pre-chilling, the seeds were sown in glass rhizoboxes in the greenhouse. The glass rhizoboxes and racks used in this study were designed by Bertelkamp

Automation Inc., Knoxville, TN; the framing was produced by 80/20 Inc., Columbia City, IN; and the panels were made by the University of Georgia's Instrument Shop, Athens, GA. Each box consists of two clear ¼-inch Lexan panels measuring 350 mm in length x 425 mm wide, secured with aluminum framing with drainage holes at the bottom. Each rack holds 10 boxes at a 45-degree angle. Each box was placed in a metallic bubble mailer to occlude light from the root systems (Fig. 1). Before sowing seeds, the soil was amended with lime to increase the pH to 6.5-7.0 using 3.2 grams of lime per litre of soil. To improve visual contrast for root imaging, 10% biochar was used (25 g biochar per litre of soil). The seeds were sown in early June. 1-2 g of NPK was mixed with 1 litre of water and added in the quantity of 50 mL per rhizobox every 2 weeks to promote root growth. Watering was done daily to ensure proper water use and prevent wilting/drying. Two to three seedlings per box were maintained based on seed germination percentages, and data recording was done 3 months after seedling establishment. The root traits were measured using RhizoVision Explorer [28] software based on images captured with a high-resolution camera, and they were also measured manually for overall root length, root spread, root number, root diameter, and fresh and dry root biomass. Similar data were recorded for aboveground traits, including tiller number, tiller height, tiller diameter, and fresh and dry tiller biomass.

Statistical data analyses

An analysis of covariance (ANCOVA) was used to test whether the relationship between net CO_2 assimilation (A) and stomatal conductance (g_{sw}) differed between yield classes. The model included g_{sw} as a covariate, yield class (status) as a categorical factor, and their interaction ($A \sim g_{sw} \times$ status) following the approach described by Lodge, Dijkstra [34], where A was used as a numeric response variable. All the statistical analyses were conducted using R.

Figure 1. Glass rhizoboxes showing the 3 months old seedlings established and ready for data recording on the right side. The image also shows the rhizoboxes on the left side laying in slanting position in the rack to allow the roots to grow along the glass wall.

Results

Analysis of covariance (ANCOVA) for leaf gas exchange measurements

The ANCOVA results showed that net CO_2 assimilation (A) increased with stomatal conductance to water vapor (gsw); however, the relationship between the top- and low-performing progenies differed (Fig. 2A). The output of ANCOVA obtained in Table 1 is represented as:

$$A_i = \beta_0 + \beta_1 g_{sw} + \beta_2 1(\text{Top}_i) + \beta_3 [g_{sw} \times 1(\text{Top}_i)] + \varepsilon_i$$

where β_0 is the intercept for the low-yielding group (when $g_{sw} = 0$), β_1 is the slope of A–g_{sw} relationship for the low-yielding group, β_2 is the difference in intercept between the top and low-yielding groups, β_3 is the difference in slope between the top and low-yielding groups, and ε_i is the

238 residual error term. The top-performing families showed higher carbon assimilation than low-
239 performing families, as shown in Table 1 below (ANCOVA outcome with P-value = 0.002). At
240 $g_{sw} = 0$, the model estimated an A of about 21.5 μmol m^{-2} s^{-1} for the low-yielding group, and about
241 27 μmol m^{-2} s^{-1} (21.475 + 5.50 = 26.975, rounded to 27) for the top-yielding group, as indicated
242 by the model intercept (Fig. 2A and Table 1). The slope of the A and g_{sw} relationship was steep
243 and positive in the low-yielding group whereas it was shallow in the top-yielding families (19.36
244 – 18.68 = 0.67, almost 1 μmol m^{-2} s^{-1} per 1 mol m^{-2} s^{-1}) with P-value = 0.007. This pattern suggests
245 that variation in A among low-yielding families is strongly tied to stomatal opening. While high-
246 yielding families sustain relatively high carbon dioxide assimilation and a wide range of stomatal
247 conductance (gsw), consistent with more efficient photosynthetic capacity or tighter stomatal
248 control.
249 The comparison between intrinsic water-use efficiency (iWUE = A/g_{sw}) and net CO_2 assimilation
250 (A) showed substantial variation among the progenies and between yield groups (Fig. 2B). Both
251 top and low groups spanned a broad range of iWUE values, where the highest iWUE values were
252 almost exclusively associated with the top yielding group. The upper performance envelope,
253 described by a 90^{th} percentile ($\tau = 0.90$) quantile regression [35] declined slightly with increasing
254 A, indicating a trade-off in which family with very high carbon assimilation tend not to achieve
255 the highest iWUE. Most high-biomass families clustered at intermediate iWUE of about 100-300,
256 while maintaining moderate to high A, suggesting that superior biomass production in this panel
257 is associated with family that balance carbon and water conservation rather than maximizing either
258 trait alone.
259

260

A

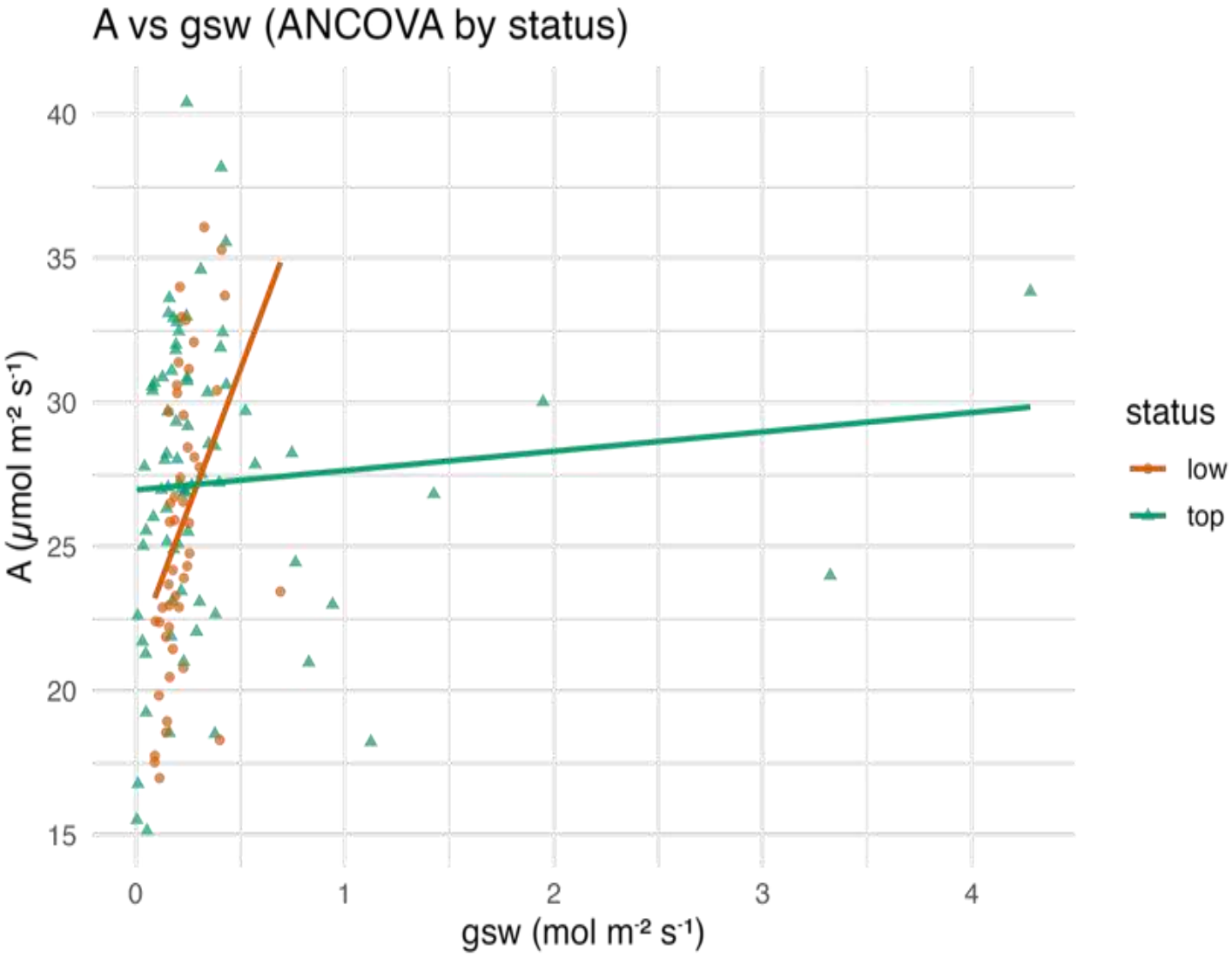
A vs gsw (ANCOVA by status)
A (μmol m⁻² s⁻¹)
gsw (mol m⁻² s⁻¹)
40
35
30
25
20
15
0
1
2
3
4
status
low
top

261

B

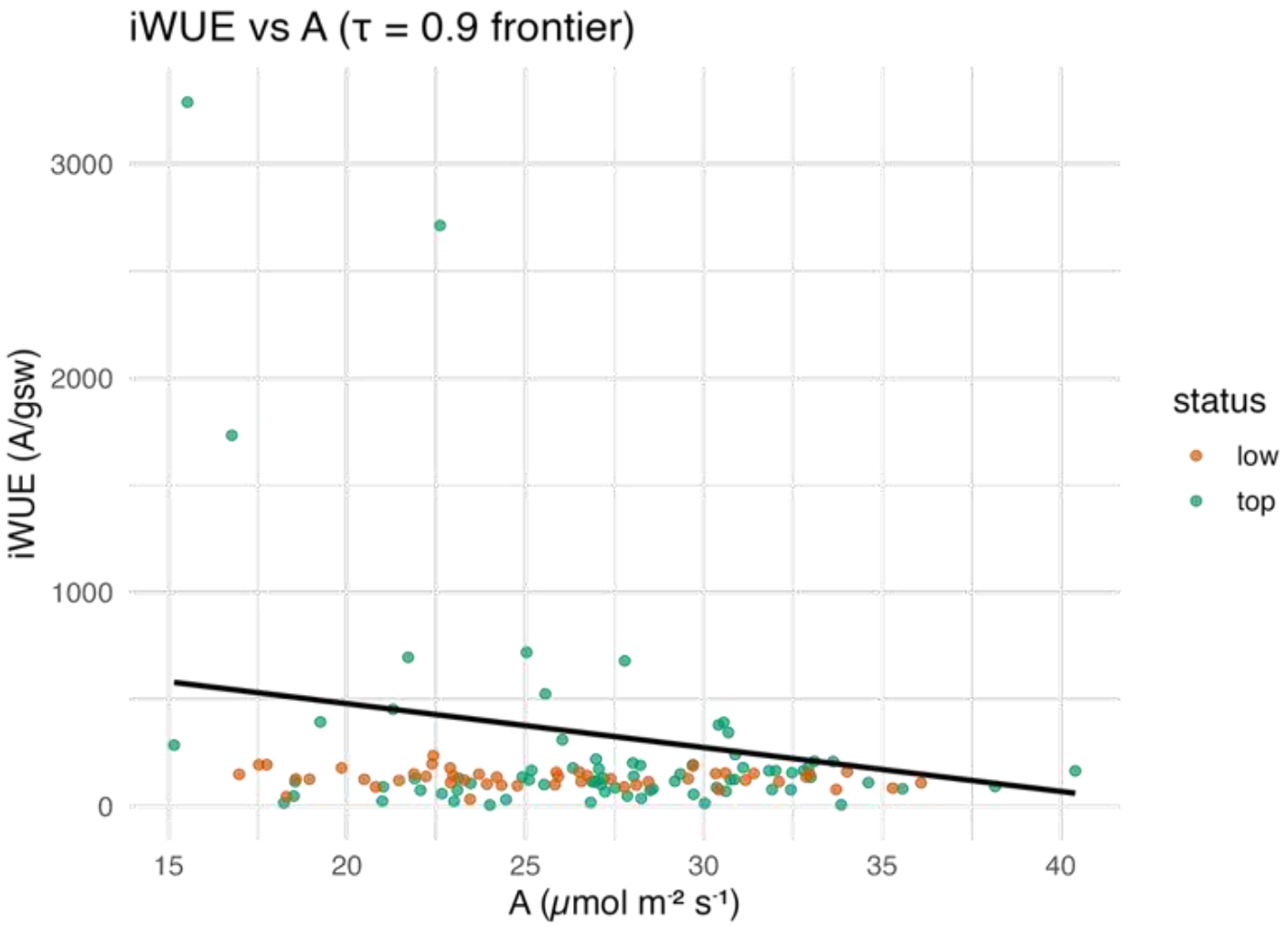

Figure 2. ANCOVA output for CO_2 assimilation (A) and stomatal conductance (gsw). (A) the graph showing the covariance of A and gsw in top and low groups. (B) Comparison of A and iWUE in top and low groups.

Table 1. ANCOVA for carbon assimilation in comparison to stomatal conductance among top- and low-yield groups.

Term	Estimate	Standard Error (SE)	Statistic (t-value)	P-value
Intercept	21.475	1.650	13.013	$1.10e^{-24}$
Stomatal conductance g_{sw} (low group slope (β))	19.356	6.756	2.865	0.00493
Yield groups (top vs. low)	5.50	1.779	3.092	0.00247
Yield groups (top and low) × g_{sw}	-18.685	6.813	-2.743	0.00703

Principal component analysis (PCA)

Principal component analysis (PCA) of the instantaneous gas exchange and microclimatic variables like CO_2 assimilation, stomatal conductance (g_{sw}), absorbed photosynthetically active radiation (PAR) and vapor pressure deficit (VPD) showed that most of the variation among plants was captured along a gradient defined by stomatal conductance and light environment (Fig. 3A). The first axis was positively associated with g_{sw} and absorbed PAR (qabs), and negatively associated with VPD, which indicated that plants with higher conductance tended to be measured under brighter, slightly less vapor-demanding conditions. The second axis contrasted high g_{sw} with VPD. The top 50 high-biomass-yielding families and the bottom 50 low-biomass-yielding families occupied largely overlapping regions of this multivariate space, with similar dispersion, suggesting the two yield groups were sampled under comparable microclimatic conditions. There was a slight shift in the high-biomass-yielding top-performing families towards the high gsw and qabs

quadrant, which showed a higher average CO2 assimilation (A); however, there was no evidence that they experienced a systematically more favorable environment than low-yielding families. The second PCA was derived using the ratios (iWUE = A/ g_{sw}, light use efficiency LUE, and the C_i/C_a) that further clarified how carbon gain and water use covaried among progenies (Fig. 3B). The first axis was positively aligned with iWUE and opposed to C_i/C_a, indicating that plants with high iWUE tended to maintain lower intracellular CO_2 relative to ambient air. The second axis was strongly associated with the LUE, separating plants that more efficiently promoted higher CO_2 assimilation using energy from absorbed light. As in the non-ratio PCA, the two yield groups overlapped, but the centroids and ellipses of the top-families extended into the region of high iWUE and LUE, and the ellipses of the low-families into the region of high iWUE, LUE and low C_i/C_a. This pattern supports the view that superior biomass production in this panel is linked to top-yielding families that combine efficient light utilization and relatively conservative stomatal behavior, rather than to differences in measurement environment per se.

A

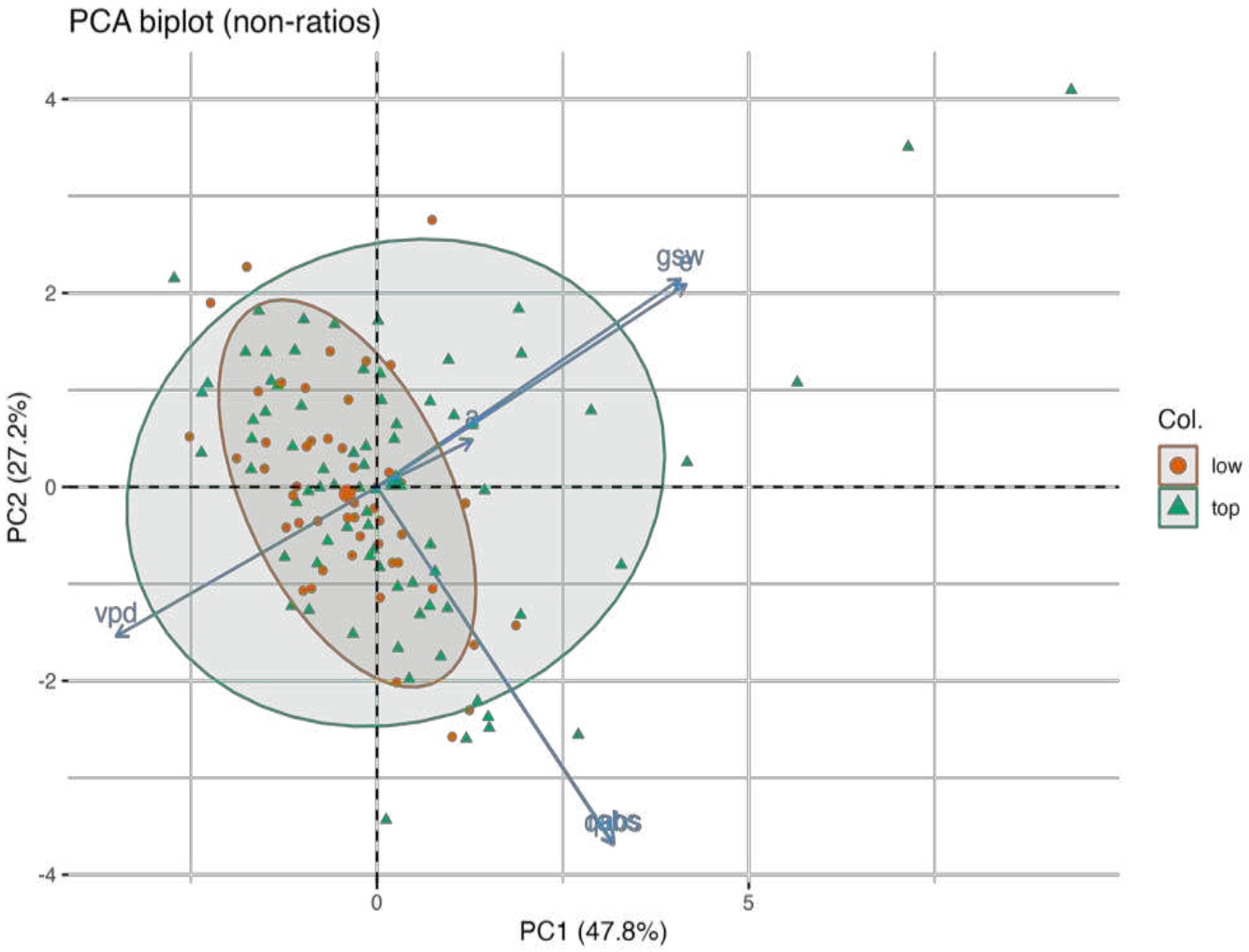
PCA biplot (non-ratios)
PC2 (27.2%)
PC1 (47.8%)
4
2
0
-2
-4
0
5
gsw
a
vpd
qabs
Col.
low
top

B

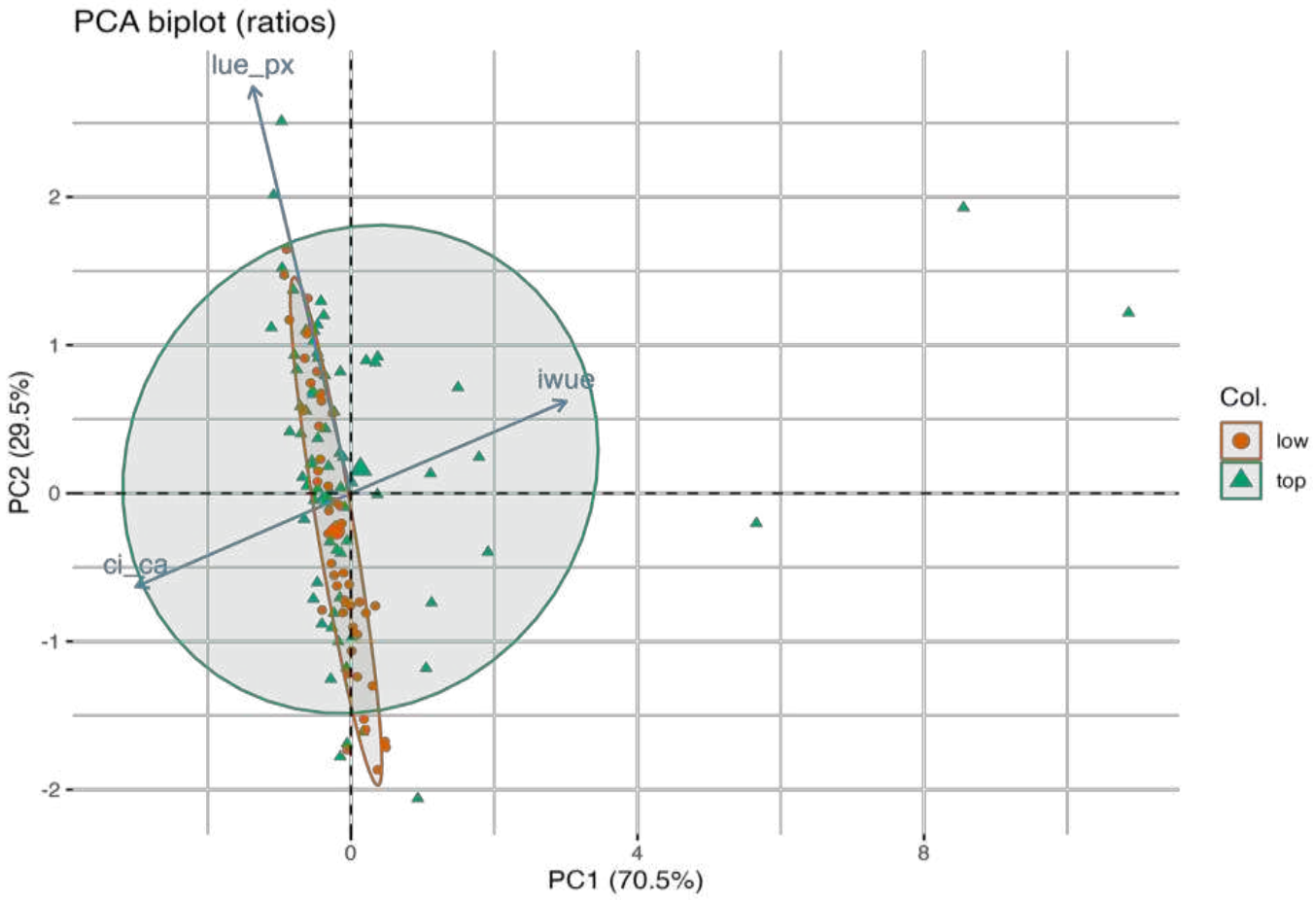

Figure 3. Principal component analysis (PCA) of leaf gas exchange measurement among top and low-yielding families. (A) PCA of non-ratio parameters showing the efficacy of carbon fixation and gas exchange among top and low-yielding groups. (B) PCA of ratios measured from LICOR.

Heatmap of gas exchange traits

A heatmap of standardized family means for the most informative gas exchange traits (C_i/C_a, g_{sw}, transpiration, VPD, iWUE and latent heat flux (LatHFlux) highlighted apparent physiological differences between the two groups of switchgrass half-sib progenies (Fig. 4). Hierarchical

clustering separated traits into two main clusters: a conductance or water loss cluster (g_{sw}, transpiration, LatHFlux, and VPD) and an efficiency cluster (C_i/C_a, and iWUE). Many of the top-yielding families showed lower-than-average C_i/C_a and strongly elevated iWUE (red boxes), consistent with a tighter drawdown of intercellular CO_2 and more carbon gained per unit stomatal conductance. In contrast, low-yielding families were enriched for near-average or higher C_i/C_a and lacked the pronounced high iWUE band observed in top-yielding families. Patterns in g_{sw} and transpiration were more heterogeneous within each status class, but several top families with high iWUE also had moderately high latent heat flux (LatHFlux), indicating that they could sustain transpiration while maintaining efficient water use. Overall, the heatmap suggested that apart from instantaneous conductance, variation in CO_2 drawdown and iWUE is a key physiological axis distinguishing top-yielding progenies from low-yielding progenies.

358

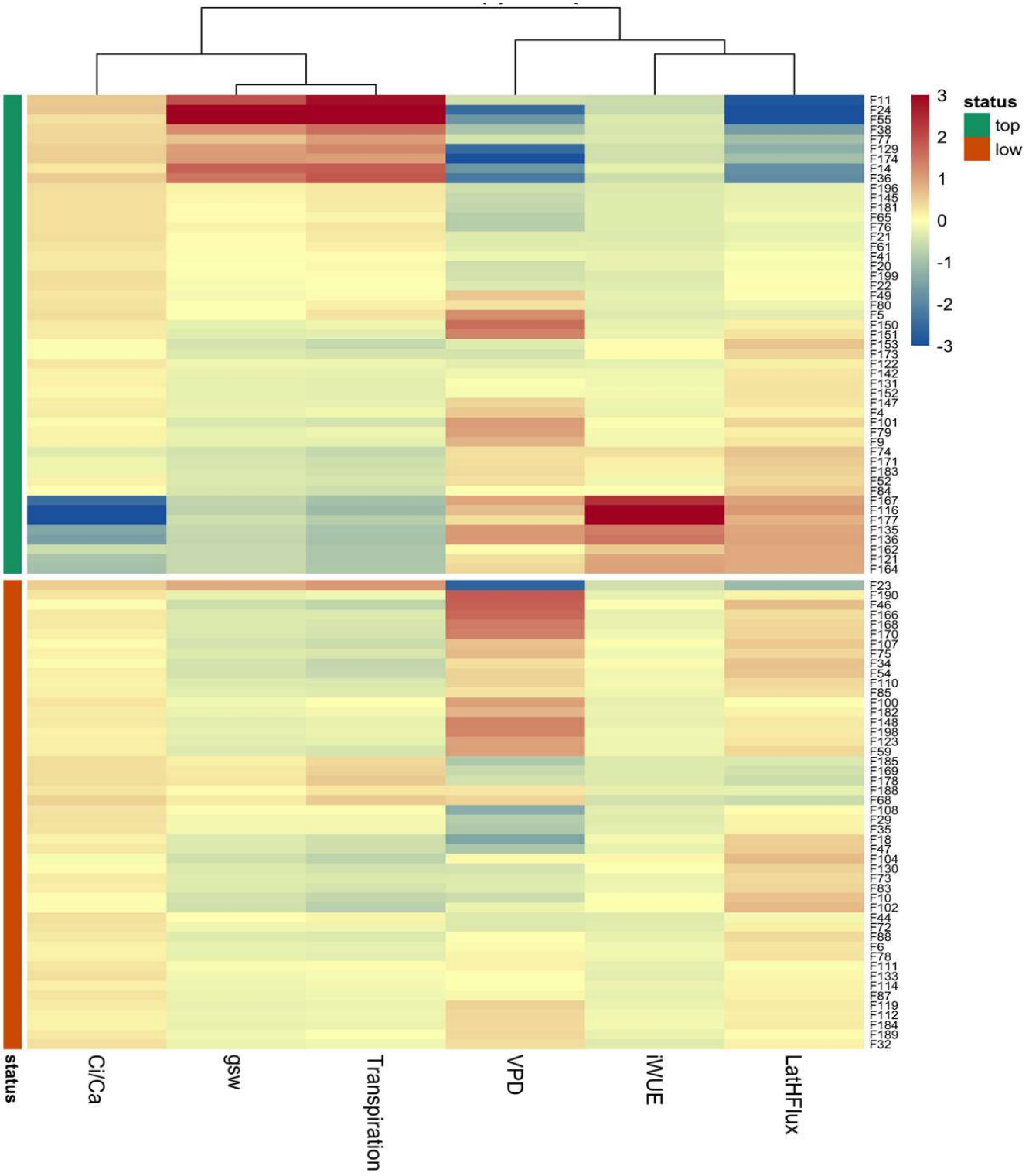

Figure 4. Heatmap of key physiological traits for gas exchange measurement among top and low-yielding progenies. Blue boxes represent weakest correlations, red boxes show strongest and light-yellow to bright yellow boxes indicate moderate correlations. LatHFlux: latent heat flux; VPD: vapor pressure deficit; g_{sw}: stomatal conductance; C_i/C_a: ratio of carbon inside leaf to atmospheric carbon.

Rhizobox experiment: root system architecture (RSA)

Correlation structure in top and low-yielding progenies

The low-yielding progenies showed a correlation pattern similar to the overall combined correlation dataset, but the relationship with mean yield across environments was negatively correlated or even absent (Fig. 5A). Fresh and dry tiller biomass were strongly correlated with the fresh and dry root biomass traits, with fresh root yield correlating with fresh tiller yield (0.72) and dry root with dry tiller yield (0.59). Mean yield remained uncorrelated with seedling root traits, with no significant correlations.

A similar pattern was observed for top-yielding families (Fig. 5B), where tiller and root biomass in seedlings were strongly correlated, but the correlation between roots and mature plant mean yield was strongly negative ($r = –0.35$ and $–0.41$). The high-yielding families thus tended to have somewhat smaller or less massive seedlings in the rhizoboxes than their lower-yielding counterparts.

This suggested that, among the top- and low-yielding groups, differences in early seedling vigor do not reliably predict variation in mature plant biomass, and that other factors, such as phenology, stress, or field establishment, likely dominated yield differences in the subset.

376

A

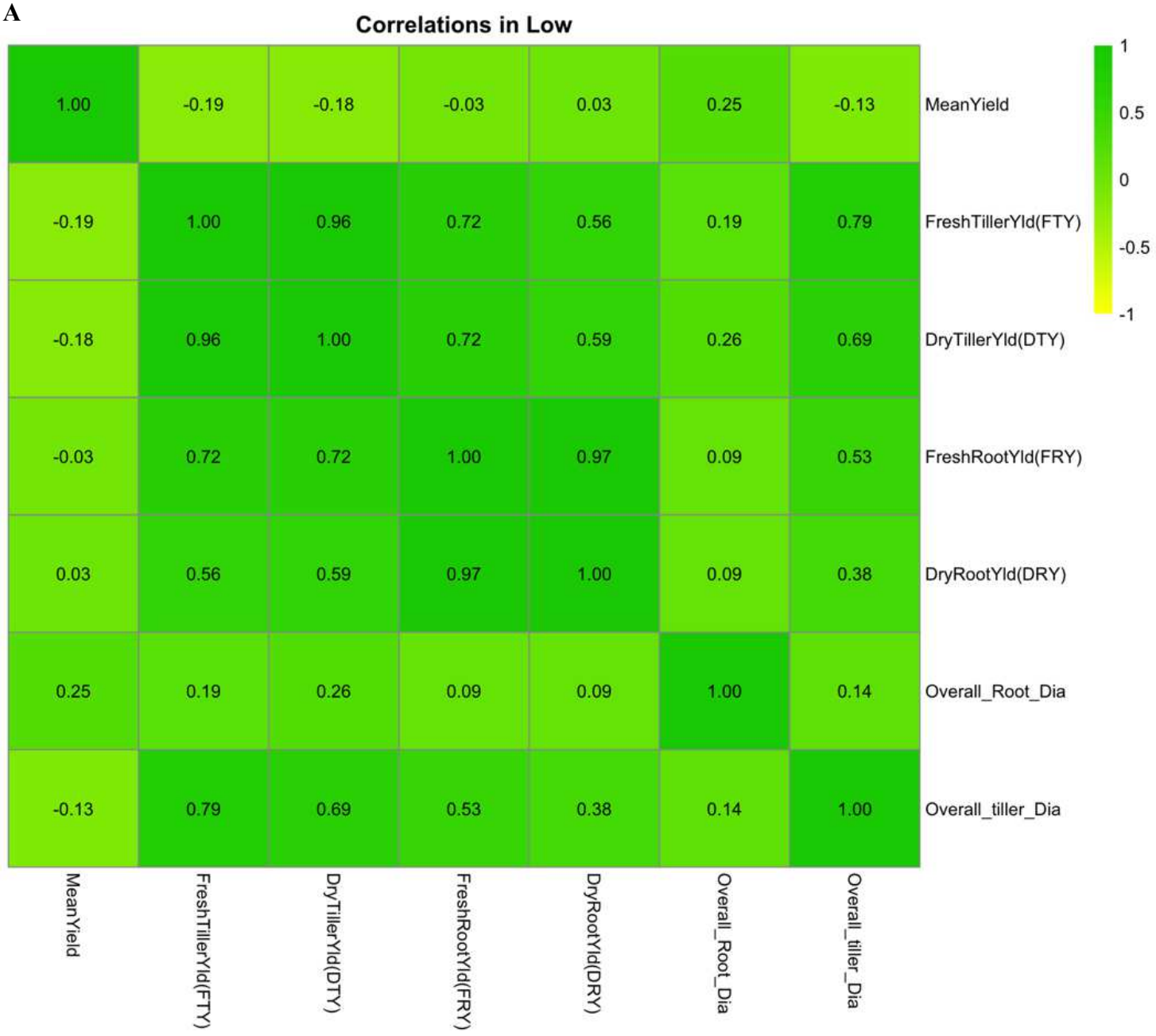
Correlations in Low
1.00 -0.19 -0.18 -0.03 0.03 0.25 -0.13 MeanYield
-0.19 1.00 0.96 0.72 0.56 0.19 0.79 FreshTillerYld(FTY)
-0.18 0.96 1.00 0.72 0.59 0.26 0.69 DryTillerYld(DTY)
-0.03 0.72 0.72 1.00 0.97 0.09 0.53 FreshRootYld(FRY)
0.03 0.56 0.59 0.97 1.00 0.09 0.38 DryRootYld(DRY)
0.25 0.19 0.26 0.09 0.09 1.00 0.14 Overall_Root_Dia
-0.13 0.79 0.69 0.53 0.38 0.14 1.00 Overall_tiller_Dia
MeanYield
FreshTillerYld(FTY)
DryTillerYld(DTY)
FreshRootYld(FRY)
DryRootYld(DRY)
Overall_Root_Dia
Overall_tiller_Dia
1
0.5
0
-0.5
-1

377

B

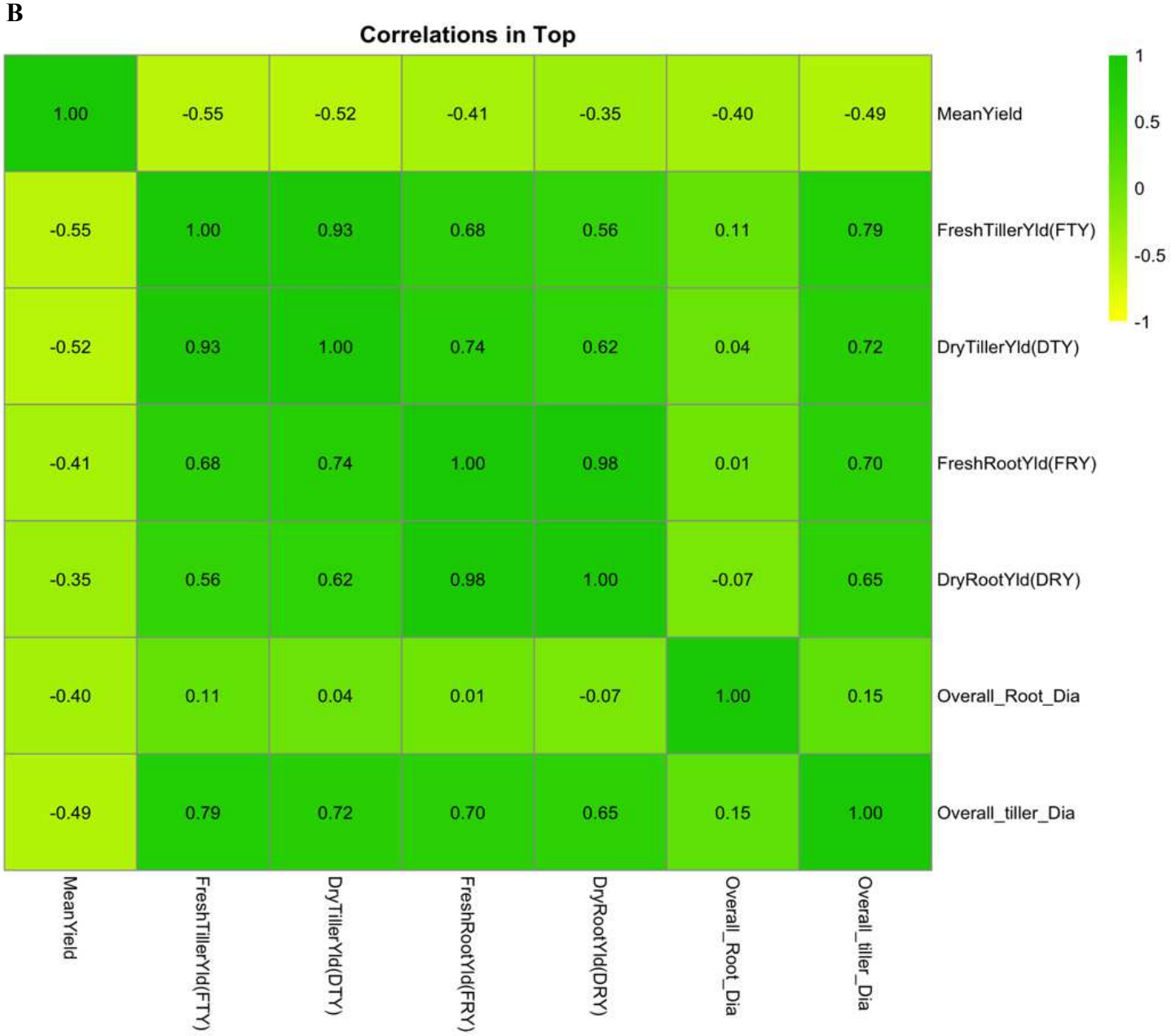

Figure 5. Pearson's correlation among top and low-yielding progenies. (A) Low-yielding progenies correlations. (B) Top-yielding progenies and their correlations.

Association of seedling root and shoot traits with field biomass

Across all 60 half-sib progenies (top 30 and low 30), seedling tiller and root biomass traits were strongly intercorrelated, whereas their association with field biomass yield across three years was weak but positive (Fig. 6). Fresh and dry tiller biomass for the seedlings showed strong positive correlations with seedling root biomass: dry root biomass correlated with dry tiller yield at 0.64, and fresh root yield correlated with fresh tiller yield at 0.72, suggesting that progenies producing more vigorous tillers at the seedling stage also accumulate more biomass below ground. With the pooling of top and low families, the correlation between mean yield across environments and root traits was positive but weak, with 0.27 for fresh root biomass and 0.31 for dry root biomass. This indicated that the pooled data is driven by between-group differences, whereas within the top families, there was evidence of a trade-off between greater seedling root biomass and mature plant yield (Fig. 5B). These correlations suggested that while early seedling biomass is internally coherent across organs, and because the study was conducted inside greenhouse, it explains only a small fraction of the variation observed in mature plant yield under field condition.

393

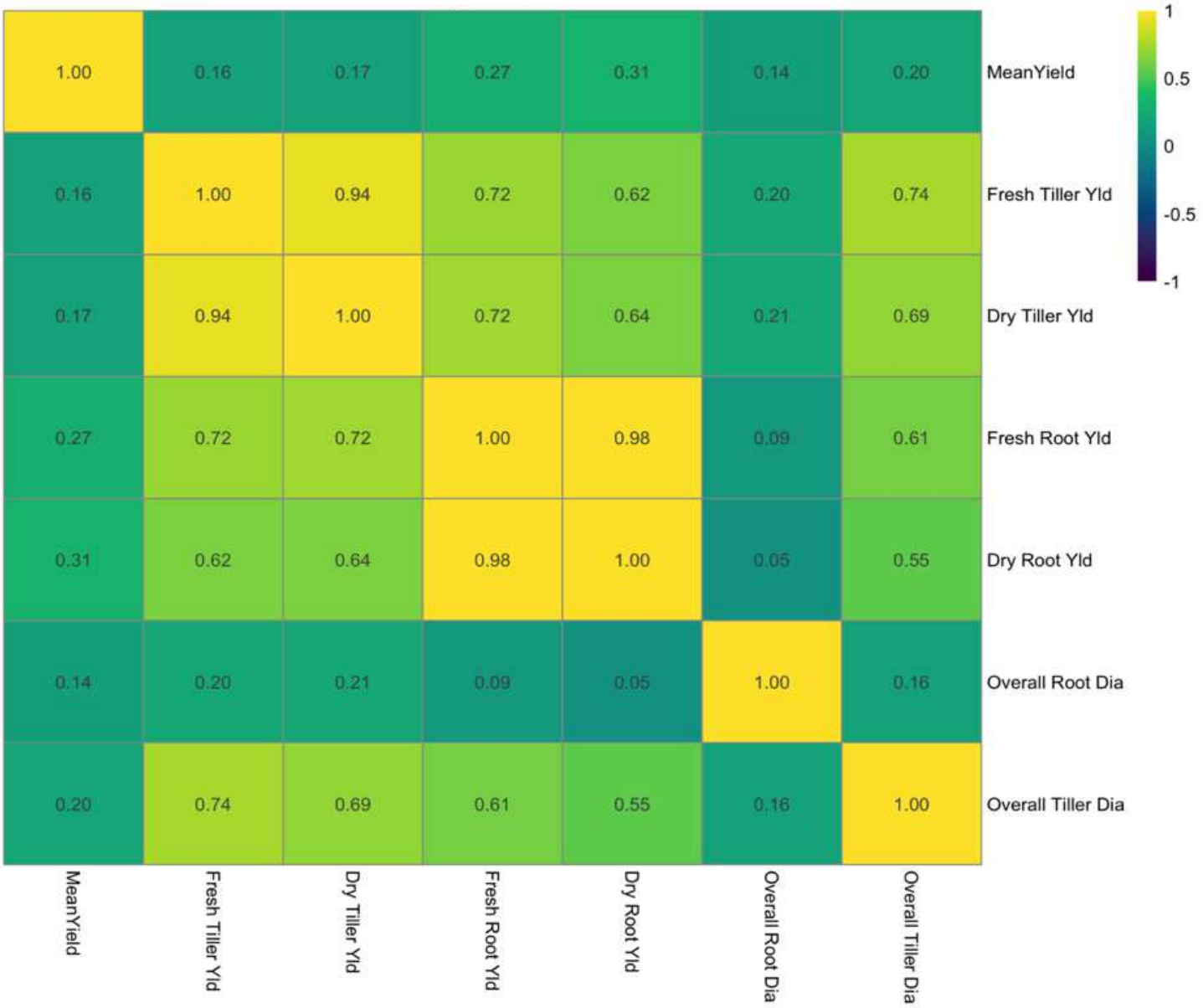

Figure 6. Combined correlation of seedling root systems among top and low-yielding progenies with mean yield across environments in mature plants and with seedling above-soil traits.

Association of RhizoVision root analysis outcomes with shoot biomass

Correlation analysis between rhizobox-derived root traits and seedling tiller characteristics revealed coordinated above and below-ground growth. The overall outcome showed a weak link with mean biomass yield in field conditions (Fig. 7). Root system size traits such as total root length, depth, maximum width, and root volume were consistently and positively correlated with tiller structural traits. The tiller diameter metrics and the fresh and dry tiller biomass yield generally ranged from $r = 0.30$ to $r = 0.60$. Root volume and surface area showed moderate correlations with both fresh ($r = 0.40$ - 0.43) and dry ($r = 0.51$) tiller yields. The maximum root width and width-to-depth ratio were similarly associated with tiller biomass and overall tiller diameter ($r = 0.33$ - 0.45).

Families with thick tillers and higher tiller biomass tended to develop root systems with larger maximum width, greater volume and surface area, and larger average root diameter. This outcome indicated that more expansive and thicker root systems support robust tillers at the seedling stage. In contrast, traits describing root angle distribution, where average root orientation and medium angle frequency were only weakly correlated with most tiller traits, with correlation in the range of $r = -0.30$ and $r = 0.10$. This suggested that variations in rooting angle were largely independent of early shoot morphology. Across all traits, correlations with mean field biomass yield were small in magnitude (≤ 0.20). These observations indicate that seedling RSA explains only a limited proportion of variation in mature biomass under field conditions.

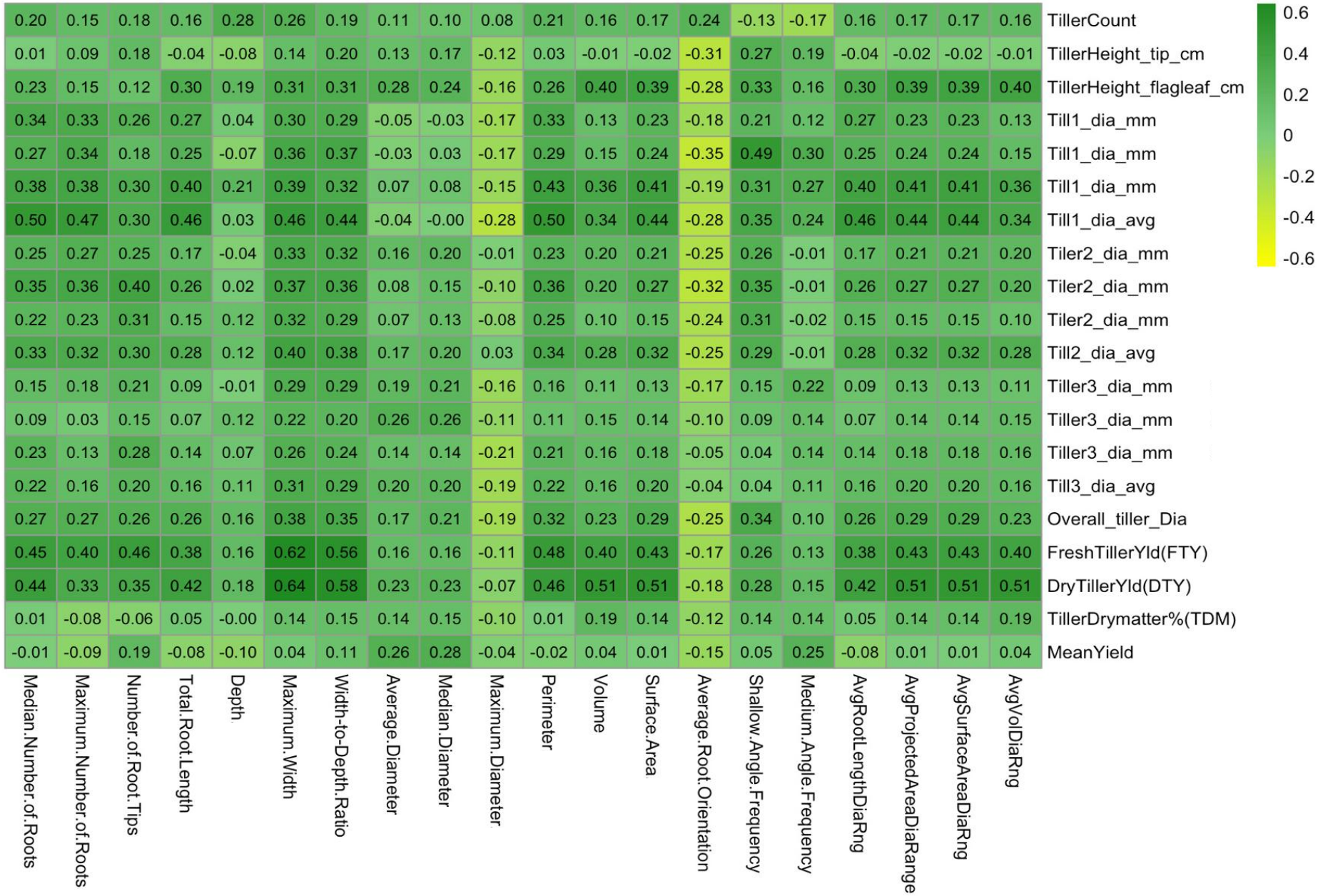

413

Figure 7. RhizoVision Explorer generated root morphological outcome correlation to manual shoot observation. The green color indicated strong positive correlation while light to medium yellowish colored boxes indicates weak negative correlation.

OJIP-derived fluorescence traits from rapid light curves

RLC slope (α) remains the same between the top and low yield groups

The initial slope (α) of the RLC was similar in both top and low yielding families (Fig. 8A). Median α was approximately 0.082 in the low-yielding group and 0.081 in the top-yielding group with interquartile ranges of about 0.080-0.086 and 0.078-0.085, respectively. The two boxplots largely overlapped, and the difference in group medians was < 0.002 units, indicating that the efficiency of light harvesting and the initial conversion of absorbed photons into electron transport was essentially conserved across yield classes.

Correlations among ETR, Fv/Fm, and PIabs

Fluorescence traits derived from RLCs were strongly interrelated (Fig. 8B and Fig. 8C). The electron transport rate (ETR) at the measurement light level was perfectly correlated with performance index (PIabs), with r = 1.00, indicating that ETR is a direct function of absorbed PAR as calculated by HANDY PEA algorithm. Consequently, the PIabs were not used as independent predictors in subsequent models to avoid collinearity. When groups were analyzed separately, the correlation between Fv/Fm and ETRs remained positive but was slightly stronger in the low-yielding families (r = 0.64) in comparison to the top families (r = 0.48). This indicated that families with higher PSII efficiency tend to support higher electron transport rates. However, in the top group, additional factors beyond Fv/Fm, such as downstream biochemistry or stomatal control, contribute to variation in ETR.

Horizontal ranked bar plots highlighted family-to-family variation in Fv/Fm within both yield groups (Fig. 8D and Fig. 8E). Across the panel, Fv/Fm values spanned roughly 0.28-0.36, with most families clustering in an intermediate range and a subset of lines falling clearly below or above this band. Families classified as having high Fv/Fm in red bars were interspersed among

both low and top yield groups, as were those with low Fv/Fm in blue bars, indicating that PSII maximum quantum efficiency alone does not fully explain differences in field biomass. Nonetheless, a small number of families combined high Fv/Fm with high yield and may represent particularly favorable ideotypes.

Relationship between Fv/Fm and ETR across yield groups

The relationship between PSII efficiency and ETR was further examined by regressing ETR on Fv/Fm for the two yield groups (Fig. 8F). In both groups, ETR increased with Fv/Fm over the observed range, with positive slopes. From Fv/Fm = 0.28 to 0.36, mean ETR increased from about 37-38 to 40-41 μmol e^{-1} m^{-2} $s^{-1,}$ corresponding to an increase of roughly 2 to 3 units in ETR across the panel. The fitted line for the low-yielding families was slightly steeper than that for the top group, consistent with the stronger Fv/Fm -ETR correlation in that subset. Taken together with the earlier gas exchange analyses, these results suggest that PSII efficiency and electron transport capacity are essential components of photosynthetic performance. The superior biomass accumulation in the top families is more strongly associated with carbon assimilation and stomatal regulation than with large differences in OJIP-based fluorescence traits alone.

453

A

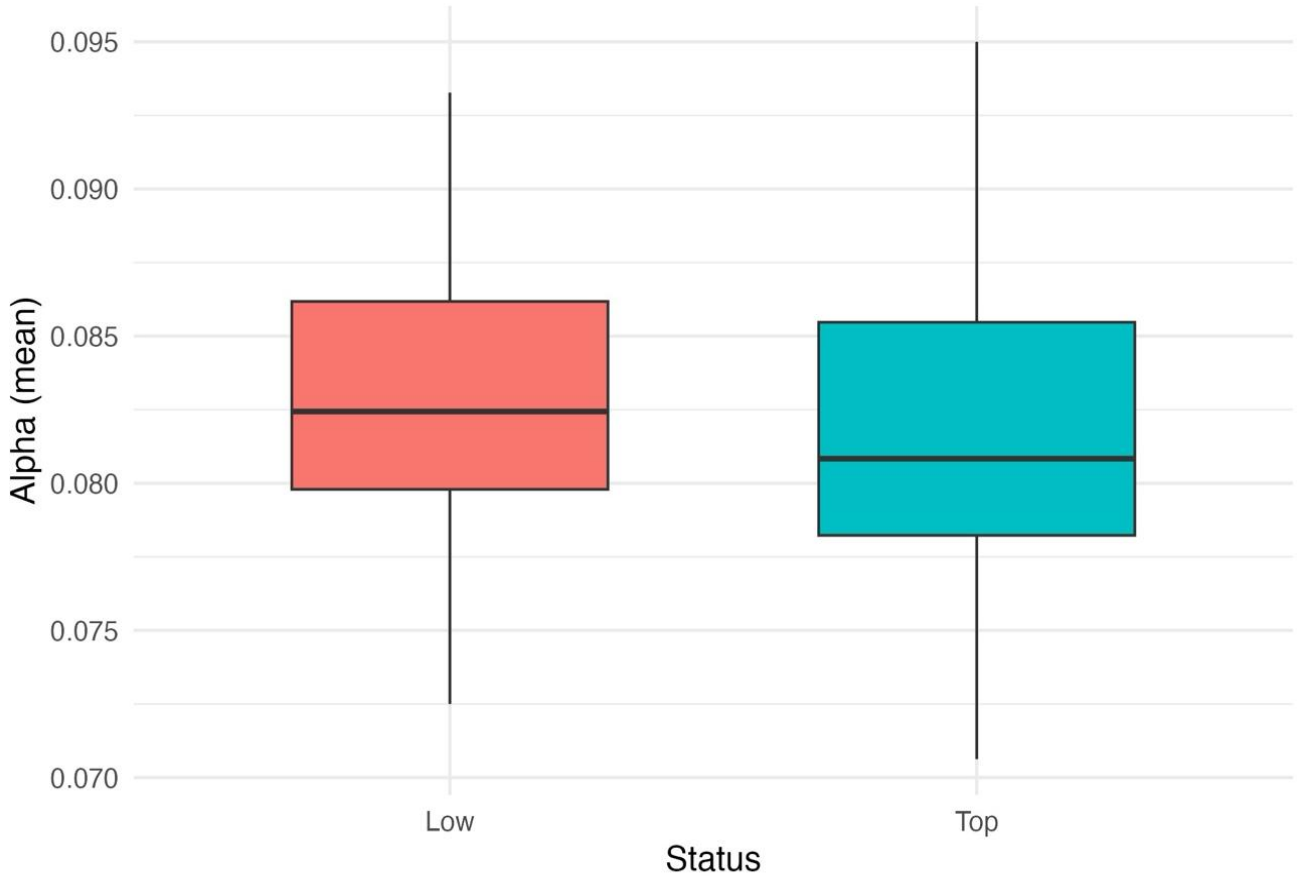

454

B

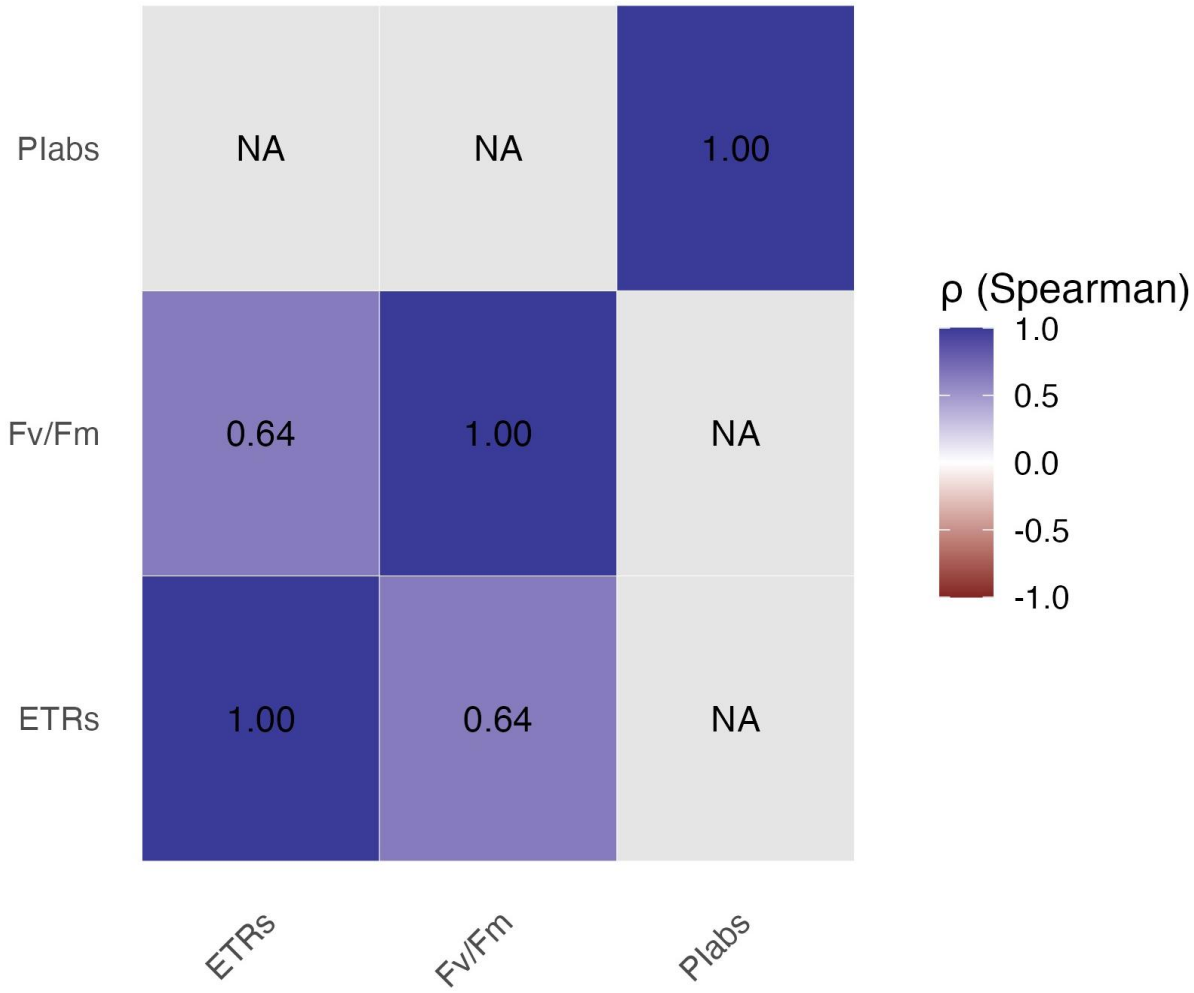
Plabs
Fv/Fm
ETRs
NA
NA
1.00
0.64
1.00
NA
1.00
0.64
NA
ETRs
Fv/Fm
Plabs
ρ (Spearman)
1.0
0.5
0.0
-0.5
-1.0

455

C

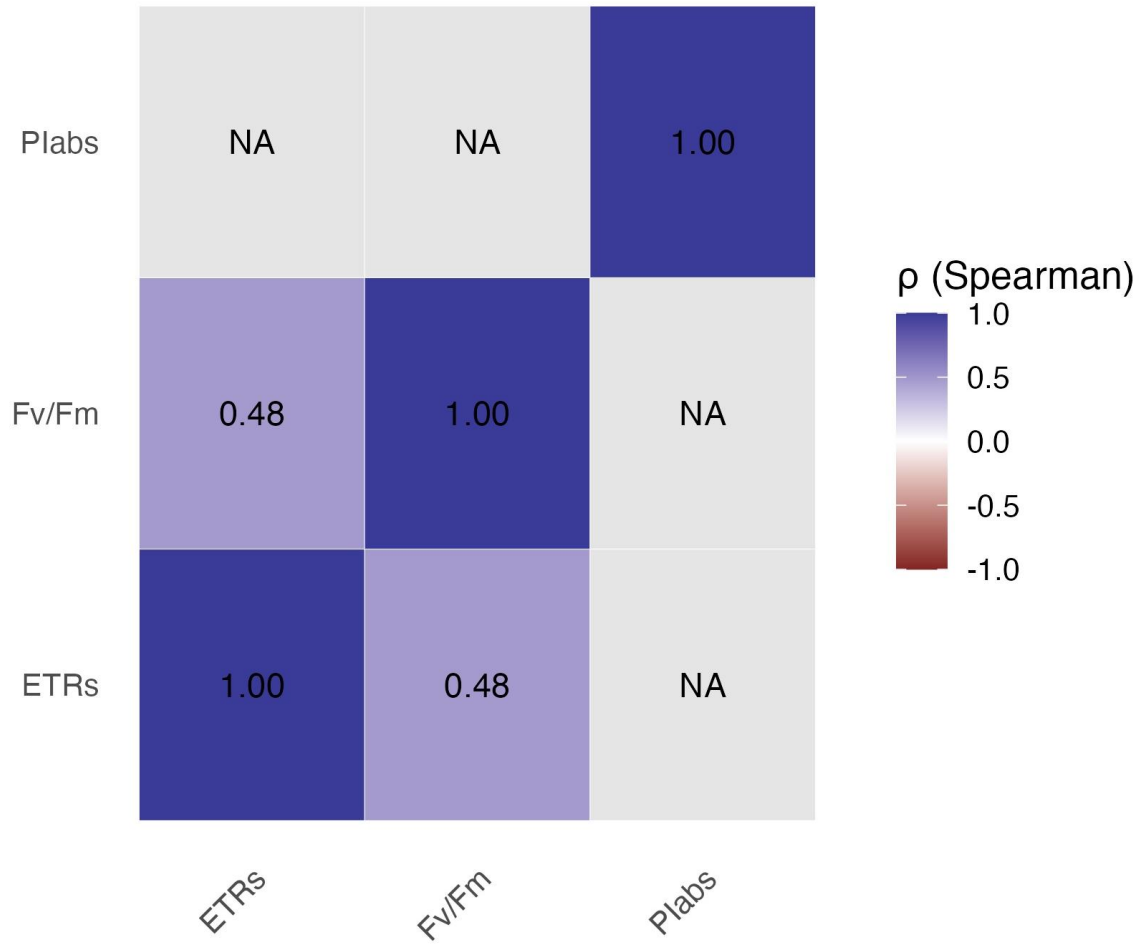
Plabs
Fv/Fm
ETRs
NA
NA
1.00
0.48
1.00
NA
1.00
0.48
NA
ETRs
Fv/Fm
Plabs
ρ (Spearman)
1.0
0.5
0.0
-0.5
-1.0

456

D

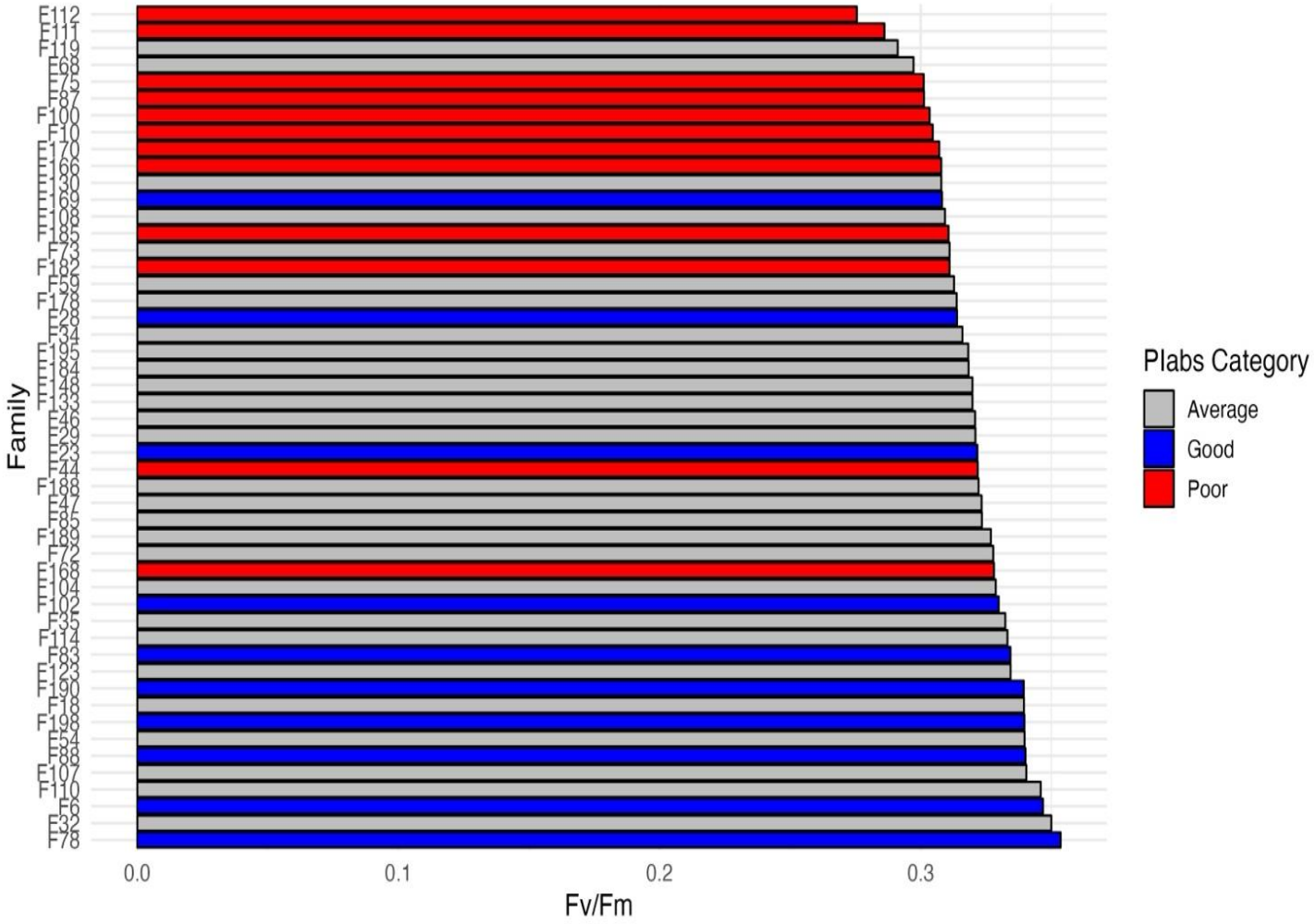

457

E

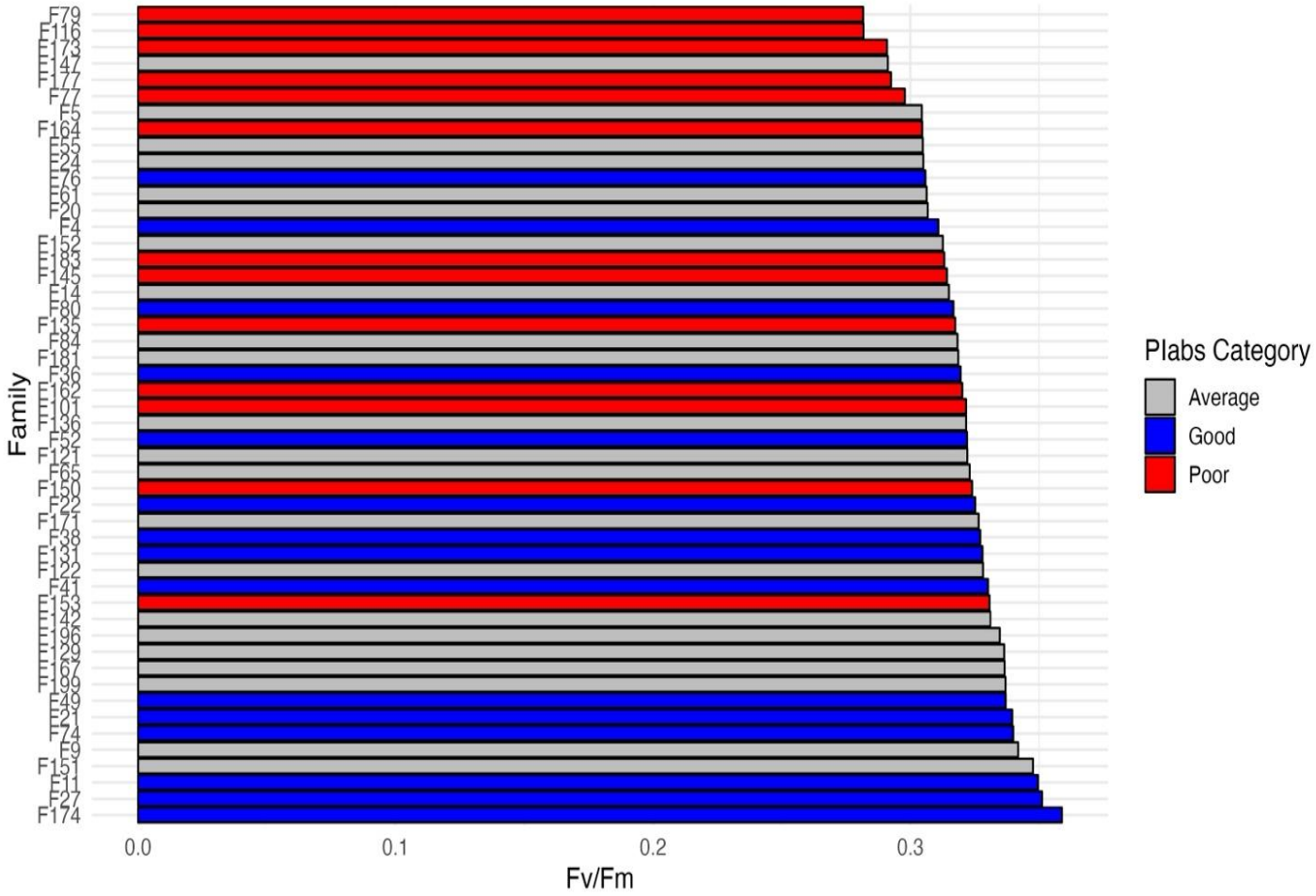
Family
F79
F116
F147
F177
F77
F164
F76
F20
F4
F145
F14
F80
F84
F181
F136
F65
F150
F171
F38
F131
F122
F41
F153
F142
F167
F199
F49
F74
F9
F151
F11
F27
F174
0.0
0.1
0.2
0.3
Fv/Fm
Plabs Category
Average
Good
Poor

45 **F**

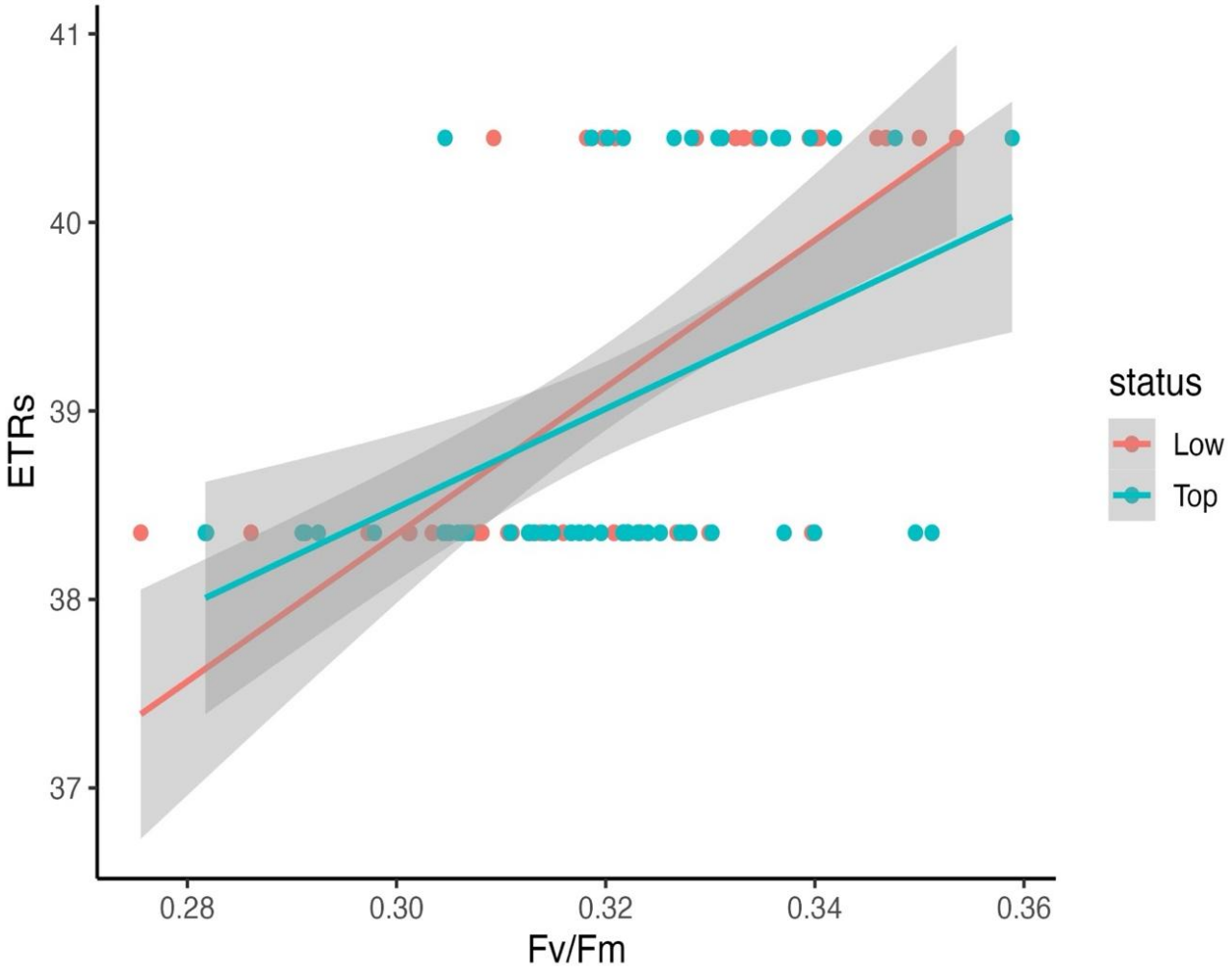

Figure 8. OJIP-derived fluorescence traits from rapid light curves recorded using HANDY PEA. (A) The graph shows the boxplots of top and low families/groups for the mean initial RLC slope (α). The pink colored boxplot indicates the low yielding family boxplot while the teal boxplot is for top yielding families. (B and C) The Spearman rank correlations (ρ) among low and top groups for electron transport rate (ETR), max photosystem II quantum efficiency (Fv/Fm), and absorbed light (Plabs). The correlations indicate strong positive correlations of Fv/Fm to ETR. (D-E) Ranking of low and top groups. The colored bars represent good, poor and average performance of families with grey bars showing average performance, blue bars show good performers and red indicate the poor performers. (F) The relationship of ETR and Fv/Fm for top and low yielding families indicating separate regression lines (pink for low and teal for top families).

Discussion

Photosynthetic regulation and intrinsic water-use efficiency

The ANCOVA of gas exchange data showed that high biomass families maintained higher net CO_2 assimilation (A) than low biomass yielding families across the observed range of stomatal conductance (g_{sw}), with a significantly shallower A–g_{sw} slope in the top yielding group (status effect P = 0.00247, interaction P = 0.00703). This pattern suggested that high-yielding progenies possess greater mesophyll or biochemical capacity for CO_2 fixation, allowing them to sustain relatively high A without proportionally increasing g_{sw}. A similar decoupling of high WUE from leaf hydraulic conductance has been reported in sorghum lines where aquaporin variation permits maintenance of photosynthesis while constraining water loss [36]. In maize, analyses of residual stomatal conductance also showed modest reductions in g_{sw} under mild water and salt stress. Stress can improve iWUE without significant penalties in A, indicating that tuning stomatal behavior around a photosynthetic capacity is a viable route to improved water economy [37].

The iWUE results reinforce this interpretation. Although both yield groups spanned a broad iWUE range, the upper iWUE envelope was largely occupied by the top families with quantile regression at $\tau = 0.90$ and the max achievable iWUE declined as A increased. This upper boundary behavior is consistent with previous studies by Liao, Gu [38], Liu, Gong [39]. Our results complement and extend previous work in switchgrass. A study of leaf-level photosynthesis at low temperatures found that genotypic differences in A did not always scale with final biomass, suggesting a context-dependent relationship between gas exchange and yield [40]. Previously, stand-level measurements comparing fertilized and unfertilized switchgrass showed limited treatment effects on leaf gas exchange parameters even when stand transpiration and productivity diverged, underscoring the complexity of linking leaf traits to whole-canopy performance [41]. Broad

examinations of WUE dynamics indicate that leaf-level WUE often increases with moderate irrigation reduction but can decline when water deficit becomes severe, reflecting non-linear feedbacks among stomatal closure, photosynthesis and evaporative demand [42]. Modelling work on highly productive perennial grasses further suggests that gains in modelled WUE do not always translate directly into proportional yield increases because canopy architecture and phenology modulate the relationship as reviewed by Kiniry and Kim [43]. Within this broad context, the high-biomass switchgrass families in our study appear to occupy a favorable region of trait space where carbon gain is sustained at moderate g_{sw}, yielding intermediate to high iWUE rather than extreme water conservation.

OJIP fluorescence traits with limited discrimination of yield groups

Rapid light curve (RLC) measurement showed that the initial slope (α) and maximum PSII efficiency (Fv/Fm) were broadly similar between high and low biomass families, with only modest variation among families. In our panel, the median α values were nearly identical between groups (about 0.081–0.082) with substantial overlap of interquartile ranges. The values indicated the differences in yield class that were not explained by large shifts in the initial photochemical efficiency. This agrees with the general fluorescence framework that Fv/Fm and related PSII indices are often conservative under non-severe stress and become much more diagnostic when plants experience strong photoinhibition or acute stress [44].

Within the top and low yield groups, Spearman correlations were moderate and positive for ETR and Fv/Fm (low group = 0.64, and top group = 0.48). These values indicate that PSII performance contributes to electron transport variation; however, it does not uniquely define the yield class. This interpretation can be supported by similar findings in wheat, where PSII efficiency was reported to be predictive of yield loss primarily under severe drought at critical stages when PSII

damage limits yield performance [45]. A similar study in tall fescue showed declines in PSII efficiency alongside reduced turf quality and physiological function, supporting the idea that fluorescence is most informative as a stress indicator rather than a yield-ranking trait under non-severe conditions [46]. In Miscanthus, drought stress was associated with shifts in Fv/Fm related to stress tolerance without a direct correlation with biomass [47]. Therefore, under mild stress, fluorescence mainly reflects a plant's momentary stress level rather than yield potential; thus, it is useful when integrated with other traits [48, 49].

Seedling RSA and relationship with mature biomass

The rhizobox root morphology experiment revealed strong coordination between root and shoot traits at the seedling stage. Across families, fresh and dry root biomass correlated strongly with fresh tiller biomass ($r = 0.59$) and dry tiller biomass ($r = 0.72$). Root size traits, for example, root volume, surface area, and maximum width, were moderately associated with tiller diameter ($r = 0.33$) and tiller biomass ($r = 0.51$). Our findings are consistent with previous studies in wheat that coupled above and below-ground growth through shared growth regulation [50, 51].

Conversely, correlations between seedling RSA traits and multi-year field biomass were weak overall (< 0.31). In the top-yielding subset, the seedling root biomass was negatively correlated with the aboveground field biomass (dry root yield $r = –0.35$, fresh root yield $r = –0.41$). These observations align with previous studies in wheat and barley where seedling root traits in controlled environments correlate poorly with field performance due to plasticity, changing trait relevance over development, and environment-specific constraints [52, 53]. Some wheat studies have found that seedling RS traits are linked to yield components under specific drought or genetic backgrounds [50, 54]. A recent study in perennial ryegrass used rhizoboxes to examine early root traits and showed that root length has a positive genetic correlation with biomass yield [55]. In a

previous study on switchgrass, yield was found to be effectively explained by composite traits related to height, phenology, leaf nitrogen content, and root traits. The study showed that traits used for yield prediction were stronger during the establishment period and during drought years for prediction, however the predictive ability declined after stand maturation [56]. That kind of shift supports our findings that RSA in our study did not track multi-year field biomass. To support the early root traits and their correlation with yield, a study in sorghum reported that RSA traits had limited predictive ability during the pre-flowering stage and higher predictive ability at the post-flowering stage for grain yield, which supports our finding of a negative correlation between RSA and field biomass in the early stages of root establishment [57].

Our integrated gas exchange and RSA results echo broader patterns seen in other perennial forage and bioenergy grasses. Tall fescue and other perennial forages can increase carbon and nitrogen and show strong yield stability, yet the relationship between below-ground and aboveground yields can vary across environments and management [58, 59]. This is consistent with the general principle that biomass production in perennial grasses (maize, Sorghum and switchgrass) is an integrated outcome of canopy development, phenology, root activity, and seasonal water balance, therefore, single traits rarely show stable high predictive power across contexts [60, 61].

Implications for breeding and functional phenomics

From the perspective of biomass breeding for bioenergy, these physiological signatures provide actionable targets for improving biomass stability and water productivity in large-scale switchgrass production systems. The results of this study suggest that leaf-level traits reflecting carbon gain under comparable stomatal opening (high A at similar g_{sw} and favorable iWUE-A combinations) may provide more consistent physiological signals of biomass potential than seedling RSA measured in controlled rhizoboxes. This framing is consistent with functional phenomics concepts

551 in which trait networks and multivariate signatures often outperform single-trait predictors when
552 phenotypes are context-dependent [39, 51]. In practice, our data support leaf gas exchange as a
553 high priority phenomics layer treating rhizobox RSA as complementary information on allocation
554 and early vigor rather than a stand-alone selection criterion.

555 **Limitations and future directions**

556 Gas exchange and fluorescence measurements provide an overall picture of biomass over a season
557 at a single location. Repeated sampling across stress gradients would strengthen inference about
558 the stability of trait differences. This is consistent with broader fluorescence and WUE studies that
559 emphasize sensitivity to environment and timing in pea, mint, and velvet grass by Moya, Loayza
560 [62], and in soybean by Miao, Guan [63]. Second, rhizobox assays are inherently simplified
561 relative to field soils and competition, where many studies showed that early root screening can
562 miss late-emerging predictors of yield [52, 64]. Finally, integrating these phenomics traits into
563 genomic models could quantify how much they add beyond pedigree/marker information for
564 predicting biomass breeding values, which are increasingly used in forage improvement programs
565 [65, 66].

566 **Conclusion**

567 This study shows that contrasting biomass performance in switchgrass half-sib families is
568 associated more strongly with how carbon gain is maintained relative to stomatal opening than
569 with large differences in PSII photochemical efficiency or with seedling root size measured in
570 rhizoboxes in a controlled greenhouse setting. High biomass families sustained higher net CO_2
571 assimilation (A) at comparable stomatal conductance (g_{sw}) as reflected by a higher modelled
572 intercept and a significantly weaker A–g_{sw} relationship. The iWUE patterns supported this
573 outcome, where top families disproportionately occupied the upper iWUE envelope. In contrast,

the declining upper boundary of iWUE at high A highlighted an inherent carbon-water trade-off, indicating that superior biomass is linked to balanced rather than extreme water-conservation strategies. In contrast, RLC-based OJIP analyses showed useful physiological context but did not clearly separate yield groups. The initial RLC slope (α) was nearly identical between groups, and Fv/Fm-ETR relationships were only moderately strong. This suggested that PSII performance contributes to variation in electron transport but is not sufficient to define biomass class. Rhizobox phenotyping confirmed strong root-shoot coordination at the seedling stage. The root biomass showed weak correlations and inconsistent links to multi-year field biomass. Together, these results show that leaf-level gas exchange traits especially the A–g_{sw} and iWUE-A trade-off are more promising physiological indicators of biomass rather than seedlings RSA measured using rhizoboxes. These findings provide a physiological basis for prioritizing gas exchange traits in bioenergy crop improvement programs aimed at stable biomass production across environments.

Author contributions

All the authors of this manuscript contributed to the manuscript preparation and finalization. Jazib Ali Irfan led the formal analysis, writing of original draft, data visualization, cleaning of data points, field and plot management, data recording. Dr. Shiva Om Makaju was involved in data recording, reviewing the original draft of manuscript, editing, writing, and data analysis. Dr. **Ali** Mekki Missaoui handled the work supervision, reviewing, the original draft, securing funds, providing resources, administration, management, formal analysis review, final approval of the original manuscript

Funding source

Support for this research was provided by the Center for Bioenergy Innovation (CBI), a U.S. Department of Energy (DOE) Research Center supported by the office of Biological and

Environmental Research in the DOE office of Science. Oak Ridge National Laboratory is managed by UT-Battelle, LLC, for the US DOE under Contract Number DE-AC05-00OR22725.

Acknowledgement

We would like to extend our special thanks to the graduate and undergraduate lab members of the Forage and Biomass Breeding group at the University of Georgia who helped in field management and with the field maintenance. We would like to specially thank the IHF crew for their support and providing the needful logistics.

Data availability

Data will be made available upon request.

Declarations

The authors declare no conflict of interest.

References

1. Mitchell, R., et al., *Dedicated energy crops and crop residues for bioenergy feedstocks in the central and eastern USA*. Bioenergy research, 2016. **9**(2): p. 384-398.
2. Makaju, S.O., et al., *Drought Adaptation Index (DAI) Based on BLUP as a Selection Approach for Drought-Resilient Switchgrass Germplasm*. Frontiers in Genetics, 2025. **16**: p. 1626083.
3. Mazarei, M., et al., *Variation in Biomass Yield and Cell Wall Composition in Switchgrass Natural Variants Under Two Nitrogen Regimes*. BioEnergy Research, 2025. **18**(1): p. 1-14.
4. Xu, Y., et al., *The efficiency and stability of soil organic carbon sequestration by perennial energy crops cultivation on marginal land depended on root traits*. Soil and Tillage Research, 2024. **235**: p. 105909.
5. Osei, A.K., N.V. Thevathasan, and M. Oelbermann, *Soil carbon dynamics in perennial biomass crops on marginally productive cropland in southern Canada*. Geoderma Regional, 2024. **39**: p. e00866.
6. Sutton, D.J., et al., *Soil health benefits of perennial biofuel crops on claypan soils*. Soil Security, 2025. **19**: p. 100193.
7. Wright, L.L., et al., *Switchgrass Production in the USA*, in *Promising resources and systems for producing bioenergy feedstocks*. 2011, IEA Bioenergy Task 43.

8. Griffiths, M., et al., *Interactions among rooting traits for deep water and nitrogen uptake in upland and lowland ecotypes of switchgrass (Panicum virgatum L.)*. Journal of Experimental Botany, 2022. **73**(3): p. 967-979.
9. Liu, Y., et al., *Assessment of drought tolerance of 49 switchgrass (Panicum virgatum) genotypes using physiological and morphological parameters*. Biotechnology for Biofuels, 2015. **8**(1): p. 152.
10. Samson, R., et al., *Switchgrass agronomy*. Ontario Biomass Producers Co-Operative Inc.: Markdale, ON, Canada, 2016: p. 82.
11. Hartman, J.C., et al., *Potential ecological impacts of switchgrass (Panicum virgatum L.) biofuel cultivation in the Central Great Plains, USA*. biomass and bioenergy, 2011. **35**(8): p. 3415-3421.
12. Tejera-Nieves, M., et al., *Seasonal decline in leaf photosynthesis in perennial switchgrass explained by sink limitations and water deficit*. Frontiers in Plant Science, 2023. **13**: p. 1023571.
13. Hu, Z., et al., *Profiling of water-use efficiency in switchgrass (Panicum virgatum L.) and the relationship with cadmium accumulation*. Agronomy, 2022. **12**(2): p. 507.
14. Peixoto, L., et al., *Deep-rooted perennial crops differ in capacity to stabilize C inputs in deep soil layers*. Scientific Reports, 2022. **12**(1): p. 5952.
15. Min, K., et al., *Deep-rooted perennials alter microbial respiration and chemical composition of carbon in density fractions along soil depth profiles*. Geoderma, 2025. **455**: p. 117202.
16. Woeltjen, S., et al., *Early changes in carbon uptake and partitioning moderate belowground carbon storage in a perennial grain*. Agriculture, Ecosystems & Environment, 2024. **370**: p. 109033.
17. Bresciano, D., et al., *Perennial C4 grasses increase root biomass and carbon in sown temperate pastures*. New Zealand Journal of Agricultural Research, 2019. **62**(3): p. 332-342.
18. Ontl, T. and M. Janowiak, *Grassland carbon management*. US Department of Agriculture, Forest Service, Climate Change Resource Center, 2017.
19. Zong, M., et al., *Ten-year effects of perennial cropping systems on soil organic carbon stock and stability in sandy soils: Mechanisms and biochemical drivers*. European Journal of Agronomy, 2025. **168**: p. 127639.
20. Ghannoum, O., Y.M. Al-Salman, and F.J. Cano, *Opportunities for improving intrinsic water use efficiency in C4 plants under climate change*. New Phytologist, 2025. **248**(6): p. 2656-2673.
21. Pignon, C.P., et al., *Drivers of natural variation in water-use efficiency under fluctuating light are promising targets for improvement in Sorghum*. Frontiers in plant science, 2021. **12**: p. 627432.
22. Vadez, V., et al., *Yield, transpiration efficiency, and water-use variations and their interrelationships in the sorghum reference collection*. Crop and Pasture Science, 2011. **62**(8): p. 645-655.
23. Kukal, M.S. and S. Irmak, *Interrelationships between water use efficiency and light use efficiency in four row crop canopies*. Agrosystems, Geosciences & Environment, 2020. **3**(1): p. e20110.

24. Mo, X., et al., *Prediction of crop yield, water consumption and water use efficiency with a SVAT-crop growth model using remotely sensed data on the North China Plain*. Ecological Modelling, 2005. **183**(2-3): p. 301-322.
25. York, L.M., *Functional phenomics: an emerging field integrating high-throughput phenotyping, physiology, and bioinformatics*. Journal of experimental botany, 2019. **70**(2): p. 379-386.
26. Guo, H., et al., *Functional phenomics and genetics of the root economics space in winter wheat using high-throughput phenotyping of respiration and architecture*. New Phytologist, 2021. **232**(1): p. 98-112.
27. Gill, T., et al., *A comprehensive review of high throughput phenotyping and machine learning for plant stress phenotyping*. Phenomics, 2022. **2**(3): p. 156-183.
28. Seethepalli, A., et al., *RhizoVision Explorer: open-source software for root image analysis and measurement standardization*. AoB plants, 2021. **13**(6): p. plab056.
29. Hu, J., et al., *Active Chlorophyll Fluorescence Technologies in Precision Weed Management: Overview and Perspectives*. Agriculture, 2025. **15**(16): p. 1787.
30. Zhu, L., et al., *Combining heat stress with pre-existing drought exacerbated the effects on chlorophyll fluorescence rise kinetics in four contrasting plant species*. International Journal of Molecular Sciences, 2021. **22**(19): p. 10682.
31. Rapacz, M., et al., *Is the OJIP test a reliable indicator of winter hardiness and freezing tolerance of common wheat and triticale under variable winter environments?* PloS one, 2015. **10**(7): p. e0134820.
32. Irfan, J.A., et al., *Selection and multi-environment yield stability analysis in a switchgrass (Panicum virgatum L.) half-sib panel*. Biomass and Bioenergy, 2026. **209**: p. 108885.
33. Hansatech Instruments, L., *Handy PEA System Manual*. 2017, Hansatech Instruments Ltd.
34. Lodge, R., et al., *Stomatal acclimation to increased CO2 concentration in a Florida scrub oak species Quercus myrtifolia Willd*. Plant, cell & environment, 2001. **24**(1): p. 77-88.
35. Koenker, R., *Quantile regression: 40 years on*. Annual review of economics, 2017. **9**(1): p. 155-176.
36. Al-Salman, Y., et al., *High water use efficiency due to maintenance of photosynthetic capacity in sorghum under water stress*. Journal of Experimental Botany, 2024. **75**(21): p. 6778-6795.
37. Ye, Z.P., et al., *Influences of residual stomatal conductance on the intrinsic water use efficiency of two C3 and two C4 species*. Agricultural Water Management, 2024. **306**: p. 109136.
38. Liao, Q., et al., *Mild water and salt stress improve water use efficiency by decreasing stomatal conductance via osmotic adjustment in field maize*. Science of the Total Environment, 2022. **805**: p. 150364.
39. Liu, Y., et al., *Chlorophyll a fluorescence as a tool to monitor physiological status in the leaves of Artemisia ordosica under root cutting conditions*. Frontiers in Plant Science, 2024. **14**: p. 1308209.

40. Cordero, Á. and B.A. Osborne, *Variation in leaf-level photosynthesis among switchgrass genotypes exposed to low temperatures does not scale with final biomass yield*. GCB Bioenergy, 2017. **9**(1): p. 144-152.
41. Albaugh, J.M., et al., *Gas exchange and stand-level estimates of water use and gross primary productivity in an experimental pine and switchgrass intercrop forestry system on the Lower Coastal Plain of North Carolina, USA*. Agricultural and Forest Meteorology, 2014. **192**: p. 27-40.
42. Zhou, H., et al., *The interrelationship between water use efficiency and radiation use efficiency under progressive soil drying in maize.* Frontiers in Plant Science, 2021. **12**: p. 794409.
43. Kiniry, J.R. and S. Kim, *A review of modeled water use efficiency of highly productive perennial grasses useful for bioenergy.* Agronomy, 2020. **10**(3): p. 328.
44. Bartold, M. and M. Kluczek, *Estimating of chlorophyll fluorescence parameter Fv/Fm for plant stress detection at peatlands under Ramsar Convention with Sentinel-2 satellite imagery.* Ecological informatics, 2024. **81**: p. 102603.
45. Sommer, S.G., et al., *The chlorophyll fluorescence parameter Fv/Fm correlates with loss of grain yield after severe drought in three wheat genotypes grown at two CO2 concentrations*. Plants, 2023. **12**(3): p. 436.
46. Zhang, X., et al., *Biosolids impact antioxidant metabolism associated with drought tolerance in tall fescue.* HortScience, 2012. **47**(10): p. 1550-1555.
47. Al Hassan, M., et al., *Investigating applied drought in Miscanthus sinensis; sensitivity, response mechanisms, and subsequent recovery.* GCB Bioenergy, 2022. **14**(7): p. 756-775.
48. Arief, M.A.A., et al., *Chlorophyll fluorescence imaging for early detection of drought and heat stress in strawberry plants*. Plants, 2023. **12**(6): p. 1387.
49. Xia, Q., et al., *Determination of Fv/Fm from chlorophyll a fluorescence without dark adaptation by an LSSVM model.* Plant Phenomics, 2023. **5**: p. 0034.
50. Xie, Q., et al., *Identifying seedling root architectural traits associated with yield and yield components in wheat.* Annals of botany, 2017. **119**(7): p. 1115-1129.
51. Wasson, A.P., et al., *Traits and selection strategies to improve root systems and water uptake in water-limited wheat crops*. Journal of experimental botany, 2012. **63**(9): p. 3485-3498.
52. Watt, M., et al., *A rapid, controlled-environment seedling root screen for wheat correlates well with rooting depths at vegetative, but not reproductive, stages at two field sites*. Annals of Botany, 2013. **112**(2): p. 447-455.
53. Williams, J.L., et al., *Relationships between roots, the stay-green phenotype, and agronomic performance in barley and wheat grown in semi-arid conditions*. The Plant Phenome Journal, 2022. **5**(1): p. e220050.
54. Kang, Y., et al., *Seminal root angle is associated with root system architecture in durum wheat.* Food and Energy Security, 2024. **13**(4): p. e570.
55. Malinowska, M., et al., *The value of early root development traits in breeding programs for biomass yield in perennial ryegrass (Lolium perenne L.)*. Theoretical and Applied Genetics, 2025. **138**(1): p. 31.

56. Stahlheber, K.A., et al., *Predicting productivity: A trait-based analysis of variability in biomass yield among switchgrass feedstock cultivars.* Agriculture, Ecosystems & Environment, 2020. **300**: p. 106980.
57. Magaisa, A., et al., *Linkages Between Sorghum bicolor Root System Architectural Traits and Grain Yield Performance Under Combined Drought and Heat Stress Conditions.* Agronomy, 2025. **15**(8): p. 1815.
58. Chen, J., et al., *Biomass yield, yield stability and soil carbon and nitrogen content under cropping systems destined for biorefineries.* Soil and Tillage Research, 2022. **221**: p. 105397.
59. Gregory, A.S., et al., *High-yielding forage grass cultivars increase root biomass and soil organic carbon stocks compared with mixed-species permanent pasture in temperate soil.* European Journal of Soil Science, 2022. **73**(1): p. e13160.
60. Reichmann, L.G., et al., *Inter-annual precipitation variability decreases switchgrass productivity from arid to mesic environments.* BioEnergy Research, 2018. **11**(3): p. 614-622.
61. Hostetler, A.N., S. Morais de Sousa Tinoco, and E.E. Sparks, *Root responses to abiotic stress: a comparative look at root system architecture in maize and sorghum.* Journal of experimental botany, 2024. **75**(2): p. 553-562.
62. Moya, I., et al., *Canopy chlorophyll fluorescence applied to stress detection using an easy-to-build micro-lidar.* Photosynthesis Research, 2019. **142**(1): p. 1-15.
63. Miao, G., et al., *Sun-induced chlorophyll fluorescence, photosynthesis, and light use efficiency of a soybean field from seasonally continuous measurements.* Journal of Geophysical Research: Biogeosciences, 2018. **123**(2): p. 610-623.
64. Cabeza, A., et al., *Root system architecture in a barley RIL population: Agronomic effects of seedling and adult root traits.* Field Crops Research, 2025. **324**: p. 109806.
65. Konkolewska, A., et al., *Genomic prediction of seasonal forage yield in perennial ryegrass.* Grassland Research, 2023. **2**(3): p. 167-181.
66. Nayak, S., et al., *Genetic variation for biomass yield and predicted genetic gain in lowland switchgrass "Kanlow".* Agronomy, 2020. **10**(12): p. 1845.